# IEA Common Exercise 4: ARX, ARMAX and grey-box models for thermal performance characterization of the test box

DTU Compute Technical Report-2014-08

Peder Bacher, Philip Delff
DTU Compute, Technical University of Denmark, DK-2800 Lyngby, Denmark

April 7, 2014

# Contents

# Chapter 1

# Introduction

In this report results of applying time series models for assessing the thermal performance of the IEA Annex 58 test box based on data given in the Common Exercise 4 (CE4), which was measured in Almeria, Spain. Both ARX, ARMAX and grey-box models are applied. Finally, the same models are fitted for the Common Exercise 3b (CE3) data measured in Belgium and the results are compared.

The focus in this report is on model selection and validation enabling a stable and reliable performance assessment. Basically, the challenge is to find a procedure for each type of model, which can give un-biased and accurate estimates of the essential performance parameters, including reliable uncertainties of the estimates. Important is also the development of methodologies for analyzing the quality of data, for example correlated inputs and lack of information in data (e.g. if no clear-sky days with direct solar radiation is present data), these aspects are discussed. Furthermore, new models for enhancing the description of the effect of solar radiation on the test box is presented.

# Chapter 2

# Data

In this section an exploratory data analysis is carried out to give an overview of the data used in the modelling and to point out some interesting features in the data. When the time series are re-sampled to lower sample frequency, this is carried out by taking average values in the time period. The original data is sampled every minute and e.g. 15 minutes values are calculated as the average of the series for each 15 minutes period. For a description of the data (signal names and units, see the Annex 58 Subtask 3 Common Exercise 4 instruction document (`CE4 ST3 CE4 Instruction document.pdf`).

## 2.1 Series 4

In Figure 2.1 all measurements for Series 4 are plotted, see the CE4 instruction document for further info of the variables. All series have values within an anticipated range considering the experiment setup. One particular problem with this data is that the heater is either on or off, and it is only sampled as a point value every minute, hence when re-sampled to five minutes values have approximately only 5 discrete values, which results in a poor resolution of the signal as seen in Figure 2.2. In Figure 2.3 the indoor air temperature, the external temperature, the heating and the radiation for Series 4 are plotted for a two-hours period. It is seen that the solar radiation signals are perfectly in sync.

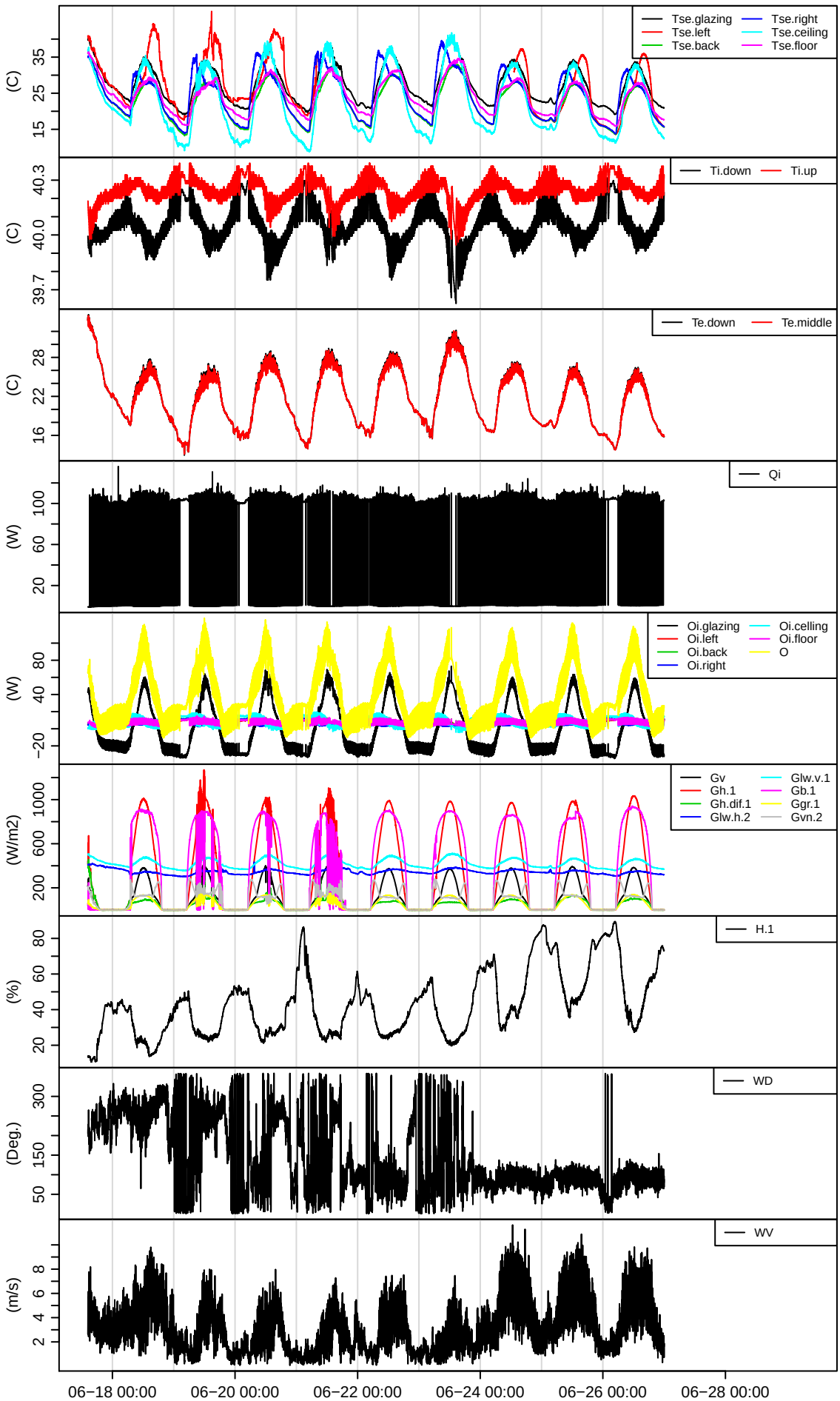


Figure 2.1: Plots of all time series in Series 4. For description of the signals and units, see the Annex 58 Subtask 3 Common Exercise 4 instruction document.

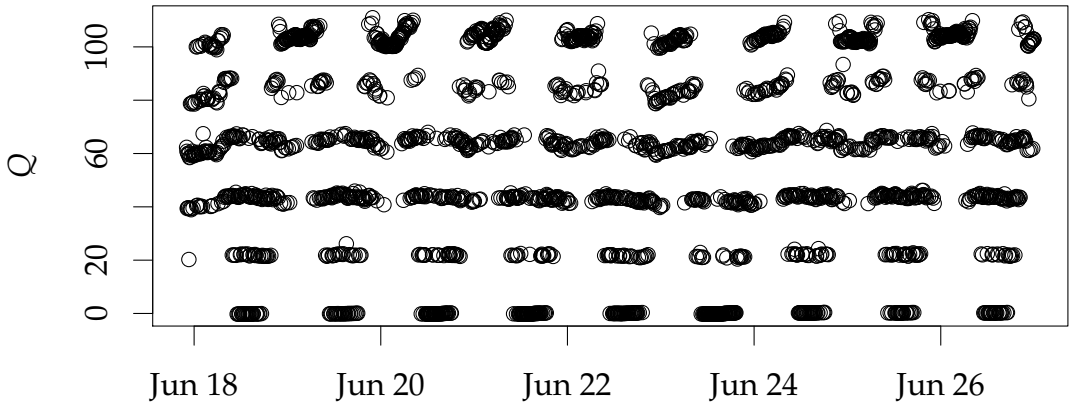


Figure 2.2: Plots five minutes values for $Q$. It can be seen that the resolution is poor, with approximately only 5 discrete values.

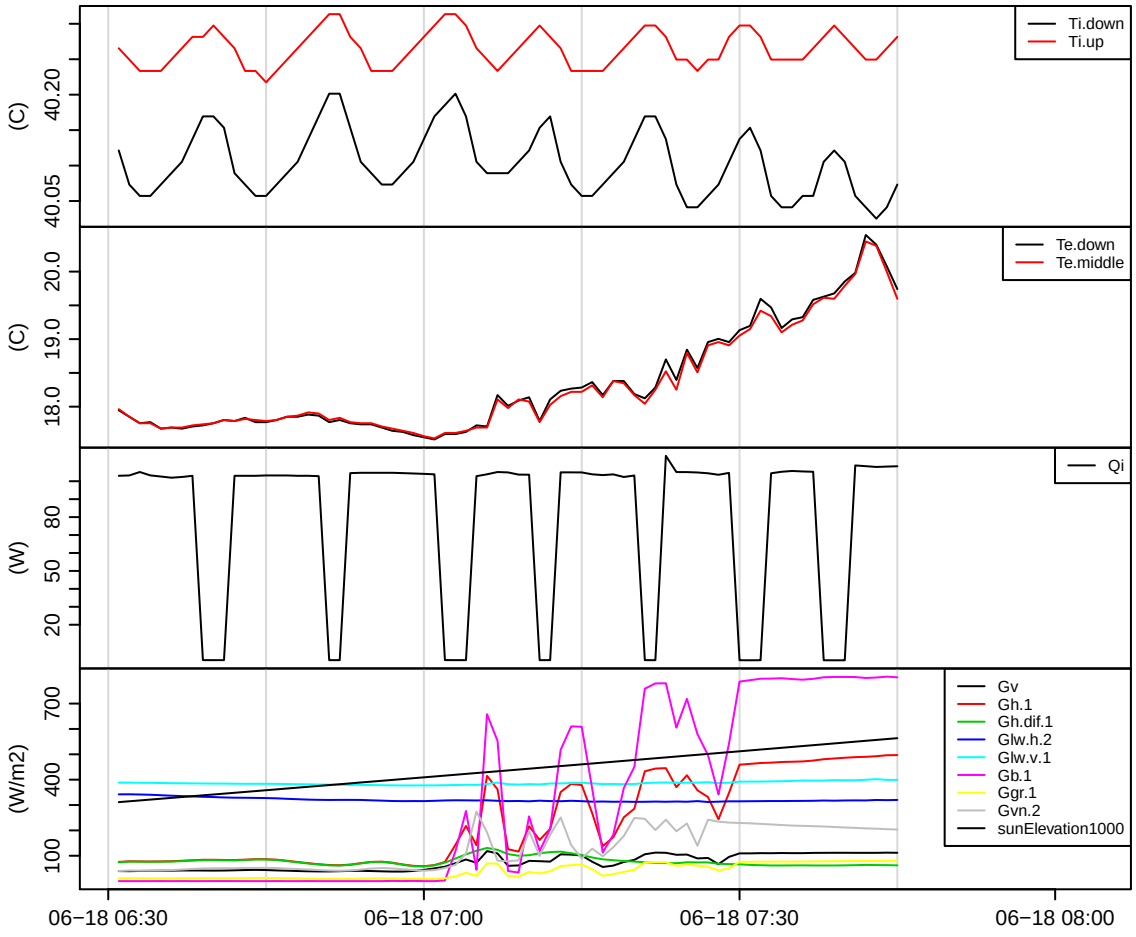


Figure 2.3: Plots of one minute values for two hours of the indoor temperature, the external temperature, the heating and the radiation for Series 4. For description of each of the signals, and units, see the Annex 58 Subtask 3 Common Exercise 4 instruction document.

## 2.2 Series 5

All the measurements from Series 5 are plotted in Figure 2.4. Again all the values are in a plausible range. The indoor temperature increase when the heaters are switched on and decrease when the heaters are switched off. From the radiation all days are with clear sky except a little cloudy drop in the last day.

In Figure 2.5 plots of the last day is seen. It is noted that when the heaters are switched off, the lower and upper indoor air temperature have different trajectory, hence a stratification occurs, which is not seen when the heaters are turned on, however the stratification is not very high. Some clouds give some fast decrease in radiation and the response in the indoor temperature can also be seen.

# Variables from the data

The following variables from the data set are used in the report. The symbols are listed for the measured variables and linked to names in the `ST3 CE4 Instruction document`. The units are the same.

Temperatures:

- $T_e$ Outdoors temperature. Taken as the average of `"Te down"` and `"Te up"` in the instructions.
- $T_i$ Indoors air temperature. Taken as the average of `"Ti down"` and `"Ti up"` in the instructions.

Heat flows and radiation:

- $Q$ or $\Phi_h$ Heating in from the heating device in the box. The `"P heating"` in the instructions.
- $G$ Global horizontal radiation. The `Gh_1` in the instructions.
- $G_{vs}$ Vertical south faced global radiation. The `Gv` in the instructions.
- $G_{vn}$ Vertical north faced global radiation. The `Gvn_2` in the instructions.

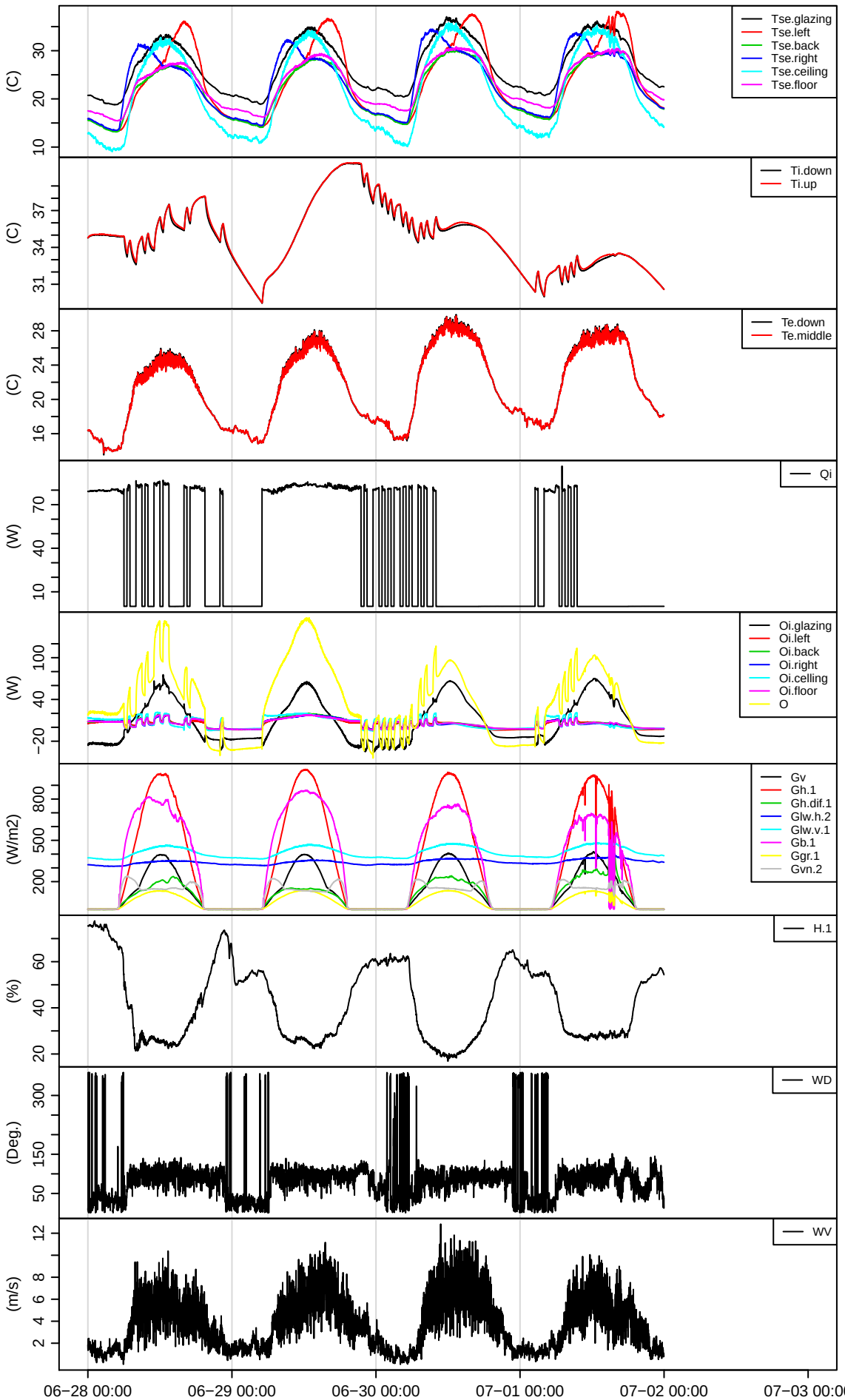


Figure 2.4: Plots of all time series in Series 5. For description of the signals and units, see the Annex 58 Subtask 3 Common Exercise 4 instruction document.

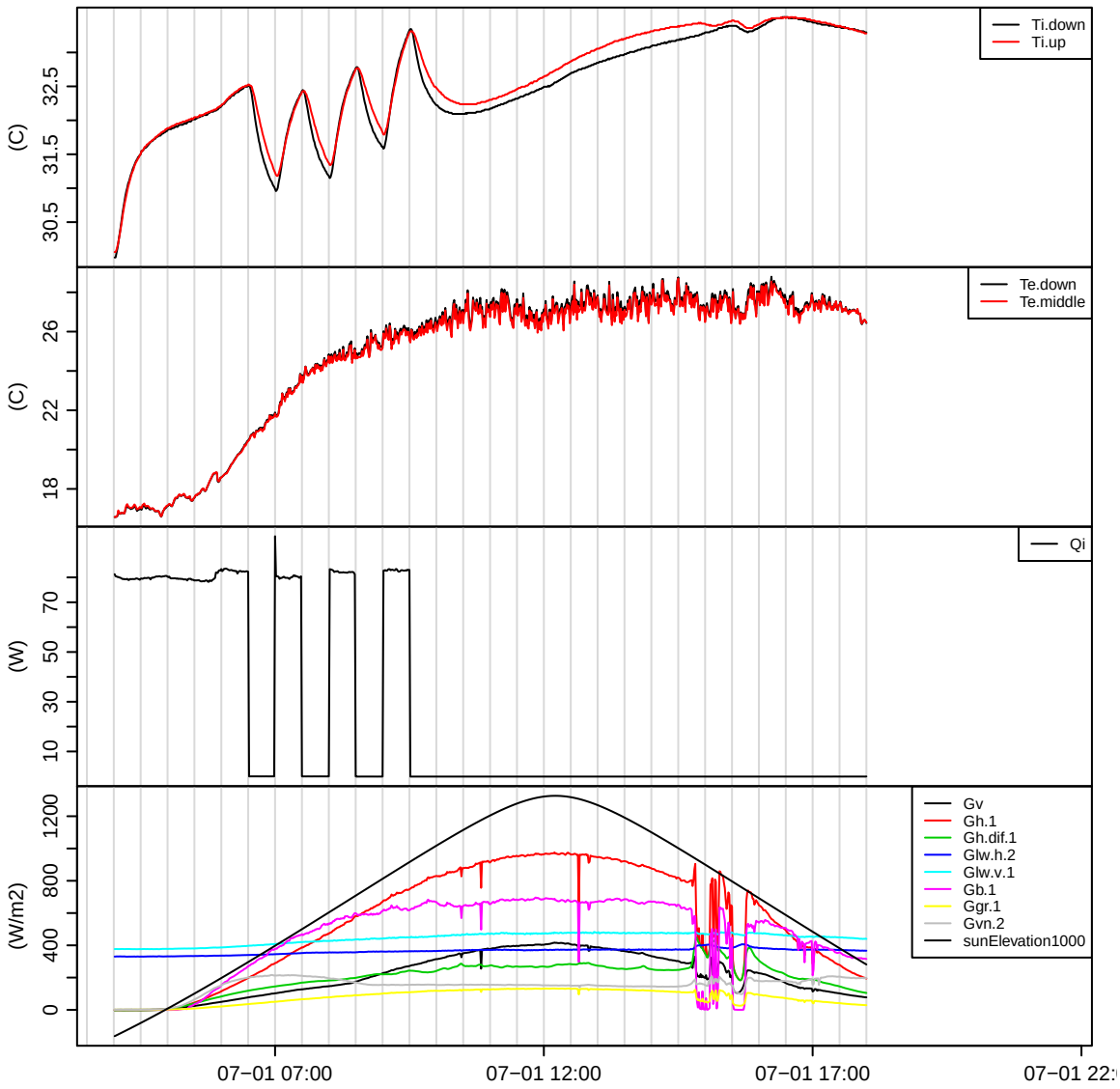


Figure 2.5: Plots of a 12 hours period of the interior temperature, the external temperature, the heating and the radiation for Series 5. For description of the signals and units, see the Annex 58 Subtask 3 Common Exercise 4 instruction document.

# Chapter 3

# ARX models

In this section the results from modelling the test box with ARX models are presented. The ARX models are fitted to the data from Series 4, which is the series with controlled heating power using a 100W incandescent lamp. Indoor air temperature set point is 40°C, dead band is 0.8°C the first day and 0.5°C afterwards. The parameters are calculated with the `lm` function in R. First a model is identified and evaluated for 30 minutes values and then a model for 10 minutes values.

The ARX models are the same as fitted in (Bacher and Delff, 2013)

$$A(q)Q_t = b_{1,0}T_t^{\mathrm{i}} + B_2(q)T_t^{\mathrm{a}} + B_3(q)G_t^{\mathrm{vs}} + \epsilon_t \tag{3.1}$$

where

$$A(q) = 1 + a_1 q^{-1} + a_2 q^{-2} + \cdots + a_{n_{\mathrm{order}}} q^{-n_{\mathrm{order}}} \tag{3.2}$$

$$B_i(q) = b_{i,0} + b_{i,1} q^{-1} + b_{i,2} q^{-2} + \cdots + b_{i,n_{\mathrm{order}}-1} q^{-(n_{\mathrm{order}}-1)} \tag{3.3}$$

where $q^{-1}$ is the back shift operator ($q^{-1}Y_t = Y_{t-1}$) and $n_{\mathrm{order}}$ is the order of the model. Hence only a single parameter $n_{\mathrm{order}}$ needs to be set, which determines the number of poles and zeroes in the transfer functions for each input, i.e. how "complex" the dynamics included in the model are. Clearly, this is a simplfied model in the sense that in theory the $B_i$ polynomials should not all nessecarily have the same order and furthermore the estimated $b_{i,j}$ cofficients are correlated and not all significant. This simplification is found to be very useful in order to make the model selection procedure easy to apply, and since only the steady-state gain of the transfer functions (i.e. the $UA$-value and $gA$-value) is used for the performance assessment an over-parametrisation has less impact of the results. A more advanced and detailed model selection could be carried out, however it was tried with no clear results.

## 3.1 ARX model selection procedure

The model order $n_{\mathrm{order}}$ needs to be set appropriately for a given set of data and sample rate, at a higher sample rate a higher model order is needed. The procedure is simply:

1. Fit the first order ARX model ($n_{\mathrm{order}} = 1$)
2. Evaluate for white noise residuals using the ACF and CCF to each of the inputs

3. If the ACF indicate that the residuals are not significantly different white noise then stop and select the model for further evaluation with time series plots

4. If the ACF indicate that the residuals are not significantly different from white noise then increase the model order with one and iterate from step 2

## 3.2 Model selection

An ARX model for 30 minutes values and an ARX model for 10 minutes values are selected.

### 3.2.1 ARX model for 30 minutes values

A model is identified for Series 4 re-sampled to 30 minutes values. In Figure 3.1 the ACF and the CCF to each input are plotted for model orders $n_{\text{order}}$ 1 to 4. The ACF of the residuals for $n_{\text{order}} = 1$ reveals a high negative correlation for lag one, hence the residuals are not white noise. For $n_{\text{order}} = 3$ all significant correlation for the shorter lags are removed, hence this model order is selected. In Figure 3.2 the inputs, the measured and predicted output, and the residuals are plotted for model order $n_{\text{order}} = 3$. No clear patterns can be observed in the residuals, hence, based on also the ACF, it is found that they are not significantly different from white noise. The model is therefore found suitable and can be used for performance assessment, for which the results are presented below in Section 3.3.

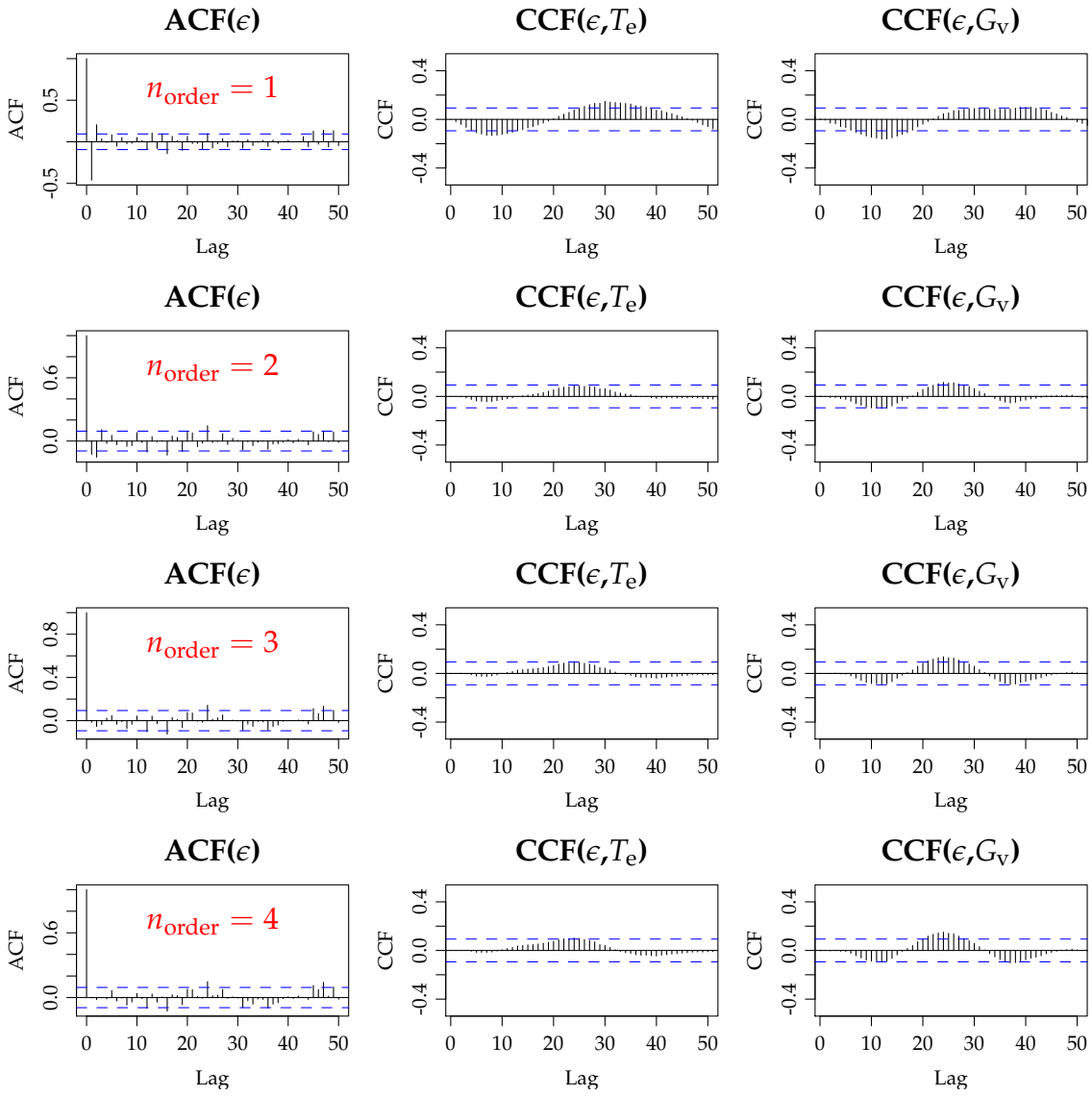


Figure 3.1: Model selection for $n_{\text{order}}$ of 1 to 4 for 30 minutes values. The ACF of the residuals and the CCF from the residuals to the external temperature and the vertical global radiation.

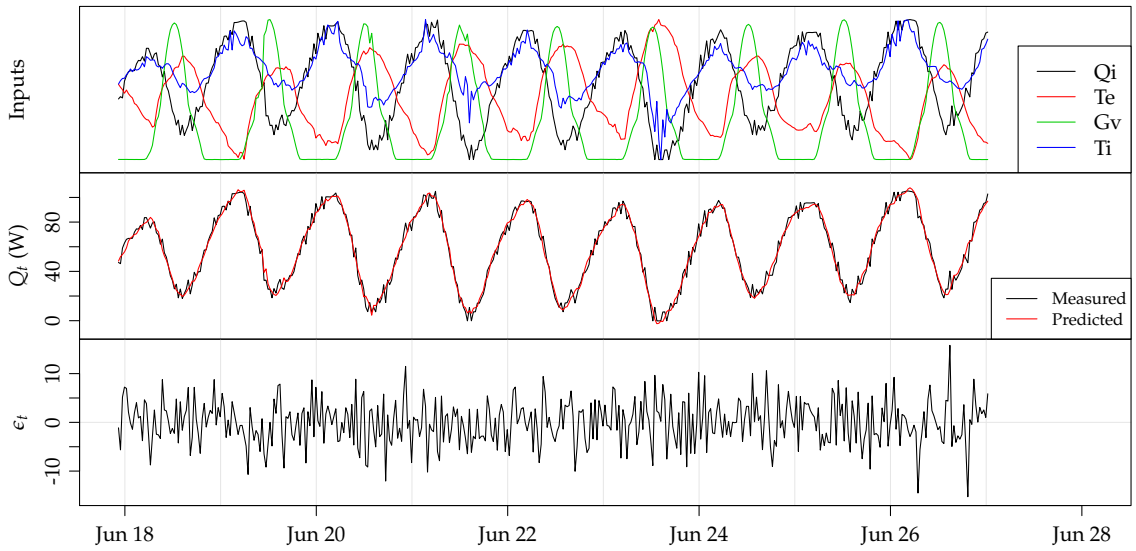


Figure 3.2: Validation of residuals for ARX model of $n_{\text{order}} = 3$ for 30 minutes values. The inputs (each normalized between min and max, hence no units) are plotted in the upper plot, the measured and predict heat load in the middle, and the residuals in the lower plot.

### 3.2.2 ARX model for 10 minutes values

For 10 minutes values the identification of an ARX model is carried out. In Figure 3.3 the ACF and CCF for the residuals are shown. At $n_{\text{order}} = 7$ the ACF shows that the residuals are not significant different from white noise and this order is used. The model is validated by considering the plots in Figure 3.4. A few short periods where the level of the residuals are lower than in other periods appear three times at night time. In these periods the heater was only sampled as 'on' and the error from only sampling the on/off heating signal every minute is therefore not present as described on page 3. Apart from these periods no clear patterns are seen in the residuals and the model order is kept.

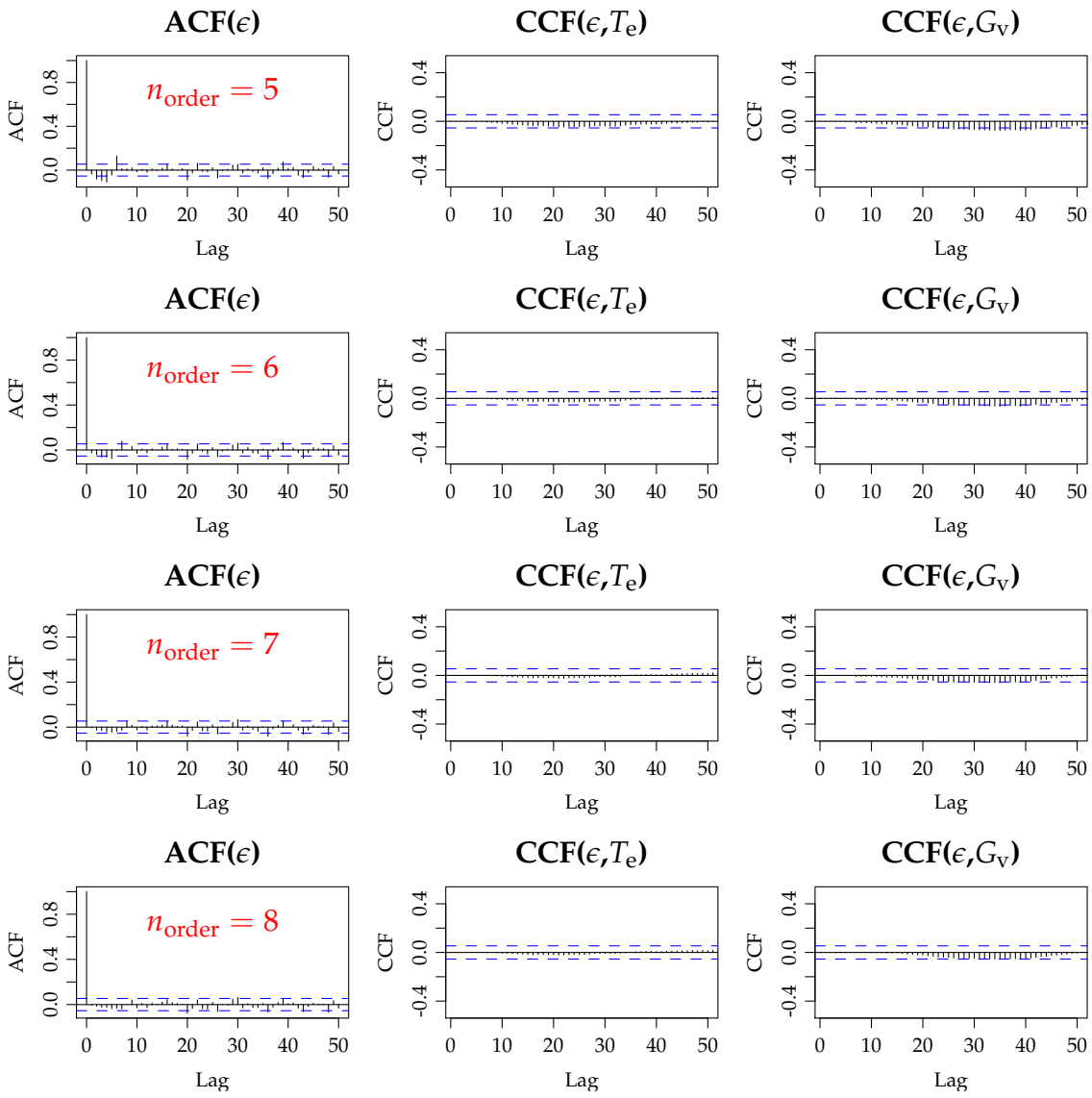


Figure 3.3: Model selection for $n_{\text{order}}$ 5,6,7 and 8 for 10 minutes values. The ACF of the residuals and the CCF from the residuals to the external temperature and the vertical global radiation.

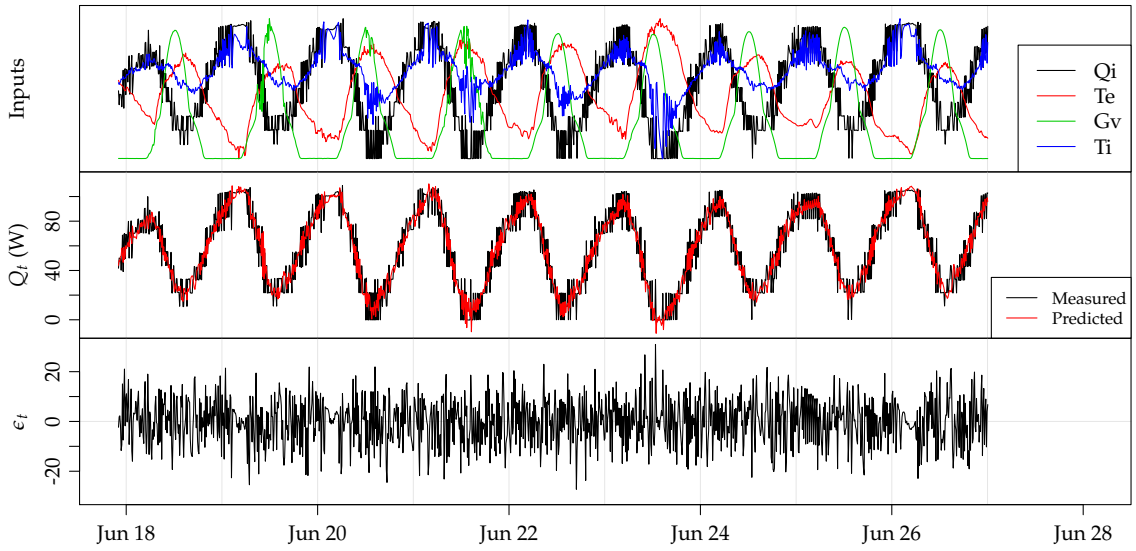


Figure 3.4: Validation of residuals for ARX model of $n_{\text{order}} = 7$ for 10 minutes values. The inputs (each normalized between min and max, hence no units) are plotted in the upper plot, the measured and predict heat load in the middle, and the residuals in the lower plot.

### 3.2.3 Models with additional inputs

The relevant inputs yet not considered were added as additional inputs one at a time to the model to see if they significantly improve the model. The following inputs did not give a coefficient estimate significantly different from zero: Vertical and horizontal long wave radiation, ground reflection radiation, wind speed and wind speed multiplied with the delta temperature (external temperature minus indoor temperature). However including the vertical north radiation gave a significant coefficient estimate and this also affects the results of the other coefficients as described in Section 6.

## 3.3 Performance assessment with ARX models

In this section the results of fitting ARX models are presented. Estimates of the *UA*-value and the *gA*-value are calculated as described in Jiménez et al. (2008) by sending a 1 through the transfer functions for the two temperature inputs and then carrying out a Lagrange weighting. Carrying out the model selection for sample periods ranging from 10 to 60 minutes the estimates listed in Table 3.1 and plotted in Figure 3.5 are found. The *UA* estimates around of 4.05 W/°C and the *gA* estimates around 0.1 $m^2$ are found reasonable from a physical perspective. Note that the estimated *gA*-value is based on the vertical global radiation measured on the facade with the window.

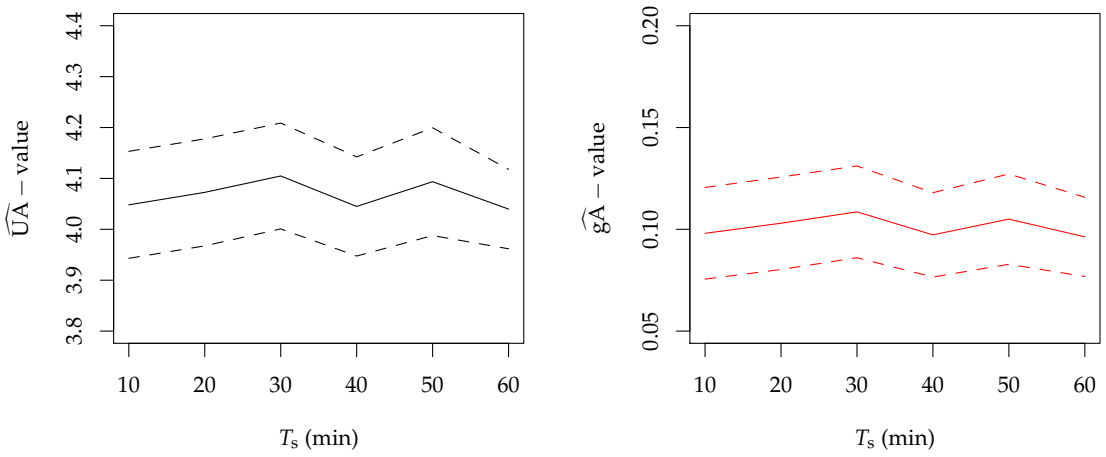


Figure 3.5: Estimates of the *UA*-value and *gA*-value found using the model selection procedure for 10, 20, 30, 40, 50 and 60 minutes values, together with the 95% confidence bounds.

| $T_s$ | $n_{order}$ | $\widehat{UA}$ | $\hat{\sigma}_{UA}$ | $\widehat{gA}$ | $\hat{\sigma}_{gA}$ |
|---|---|---|---|---|---|
| 10 | 7 | 4.05 | 0.053 | 0.10 | 0.011 |
| 20 | 4 | 4.07 | 0.053 | 0.10 | 0.012 |
| 30 | 3 | 4.10 | 0.053 | 0.11 | 0.011 |
| 40 | 2 | 4.04 | 0.049 | 0.10 | 0.011 |
| 50 | 2 | 4.09 | 0.054 | 0.10 | 0.011 |
| 60 | 1 | 4.04 | 0.040 | 0.10 | 0.010 |

Table 3.1: The *UA*-value and *gA*-value estimates for sample periods ($T_s$ in minutes) in the range of 10 to 60 minutes, together with their estimated standard deviances $\sigma_{UA}$ and $\sigma_{gA}$

# Chapter 4

# ARMAX models

In this chapter the use of ARMAX models are presented. They are applied similarly as the ARX models in the previous chapter. This is simply carried out adding an MA component to the ARX models, however this implies that the parameters cannot be calculated in close form, but has to be calculated using an iterative scheme. The `ident` toolbox in Matlab is used.

The ARMAX models are

$$A(q)Q_t = b_{1,0}T_t^{\mathrm{i}} + B_2(q)T_t^{\mathrm{a}} + B_3(q)G_t^{\mathrm{vs}} + C(q)\epsilon_t \tag{4.1}$$

where

$$A(q) = 1 + a_1 q^{-1} + a_2 q^{-2} + \cdots + a_{n_{\mathrm{order}}} q^{-n_{\mathrm{order}}} \tag{4.2}$$
$$B_i(q) = b_{i,0} \tag{4.3}$$
$$C(q) = 1 + c_1 \tag{4.4}$$

where $q^{-1}$ is the back shift operator and $n_{\mathrm{order}}$ is the order of the model. Note that the order of the $B_i$ polynomials are set to 0, this was found to give more stable estimates, this is discussed further below in Section 4.2. The order of the $C$ polynomial is set to 1.

Selection of a suitable model order $n_{\mathrm{order}}$ is carried out as for the ARX models as described in Section 3.1.

## 4.1 Model selection

In this section first a model for 30 minutes values are selected and then for the 10 minutes values.

### 4.1.1 ARMAX model for 30 minutes values

The model order needs to be determined. In Figure 4.1 the ACF of the residuals and CCF to each inputs it plotted for $n_{\mathrm{order}}$ 1, 2 and 3. From the ACF it is clear that for $n_{\mathrm{order}} = 2$ the correlation for the shorter lags are insignificant, hence this model order is selected. In Figure 4.2 the inputs, the measured and predicted output, and the residuals are plotted for model order $n_{\mathrm{order}} = 2$. No clear patterns can be observed in the residuals, hence, based on also the ACF, it is found that they are not significantly different from white noise and this model is found suitable.

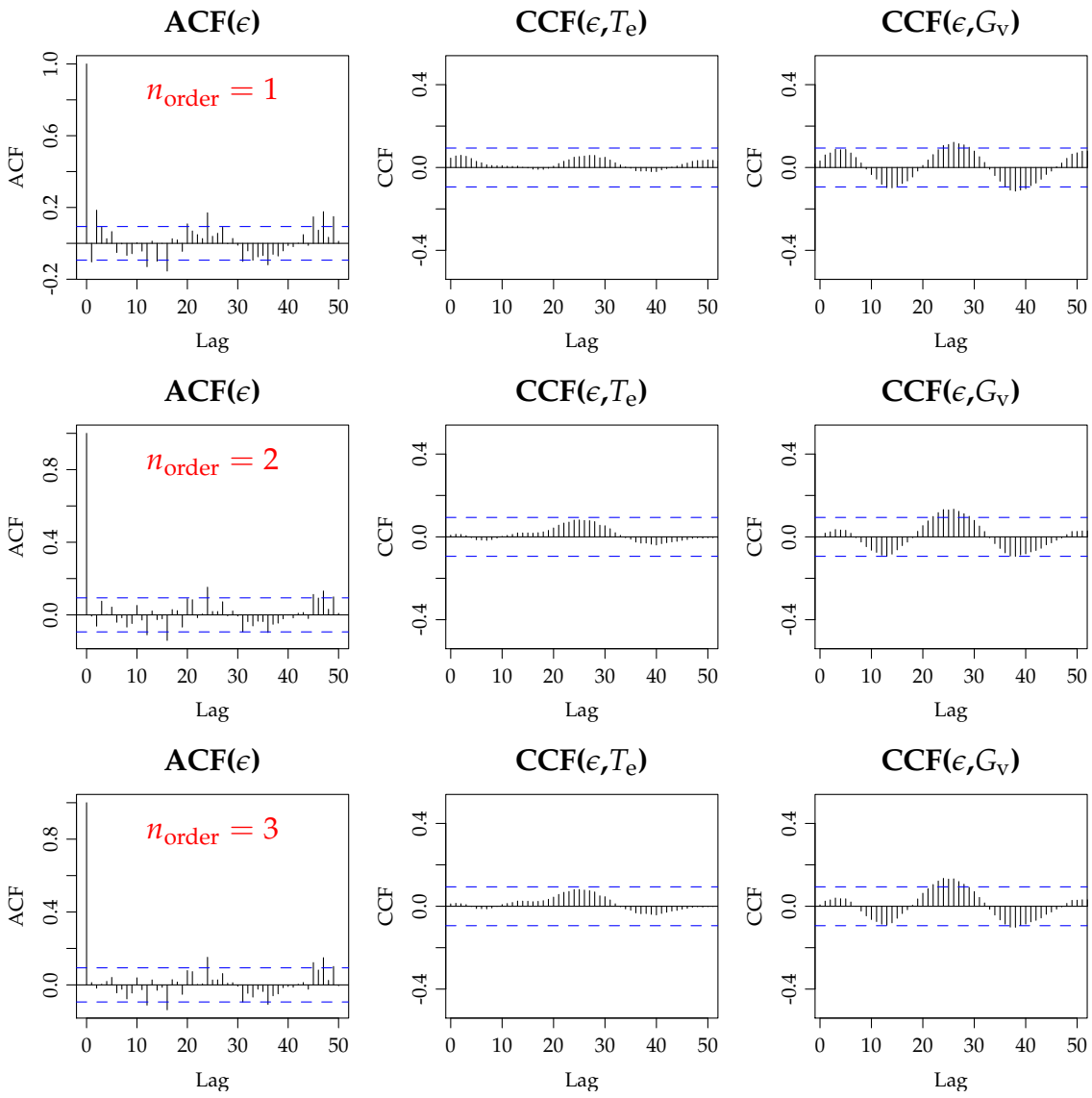


Figure 4.1: ARMAX model selection for $n_{\text{order}}$ 1,2 and 3 for 30 minutes values. The ACF of the residuals and the CCF from the residuals to the external temperature and the vertical global radiation.

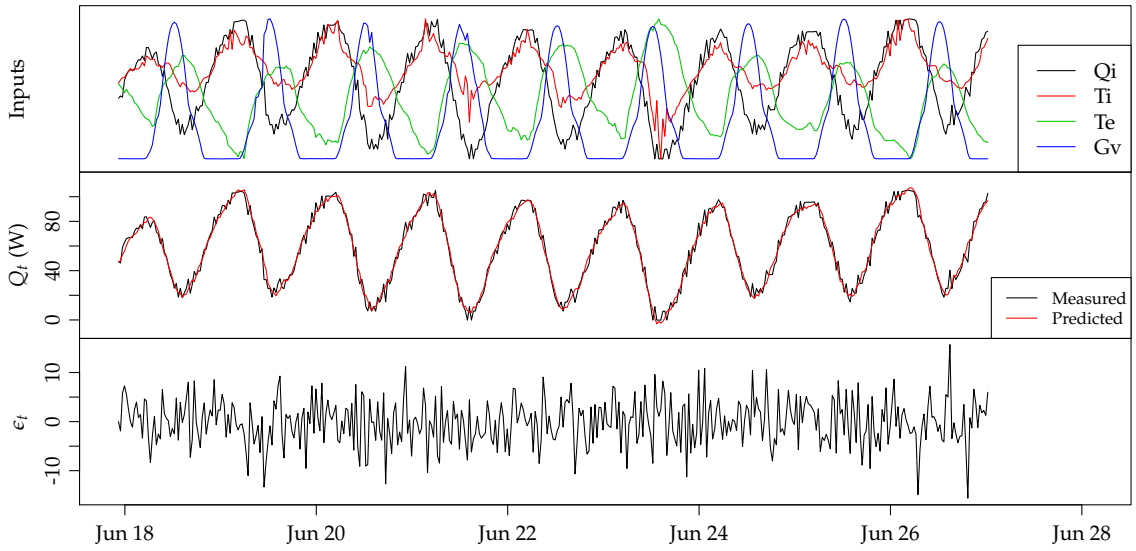


Figure 4.2: Validation of residuals for ARMAX model of $n_{\text{order}} = 2$ for 30 minutes values. The inputs are plotted in the upper plot, the measured and predict heat load in the middle, and the residuals in the lower plot.

### 4.1.2 ARMAX model for 10 minutes values

In this section a suitable model order for an ARMAX model for 10 minutes values is found. In Figure 4.3 the ACF for the residuals and the CCF to each of the inputs is plotted. At $n_{\text{order}} = 4$ the correlation for the shorter lags becomes insignificant. In Figure 4.4 no clear patterns can be observed in the residuals, hence, based on also the ACF, it is found that they are not significantly different from white noise and therefore that the model is suitable.

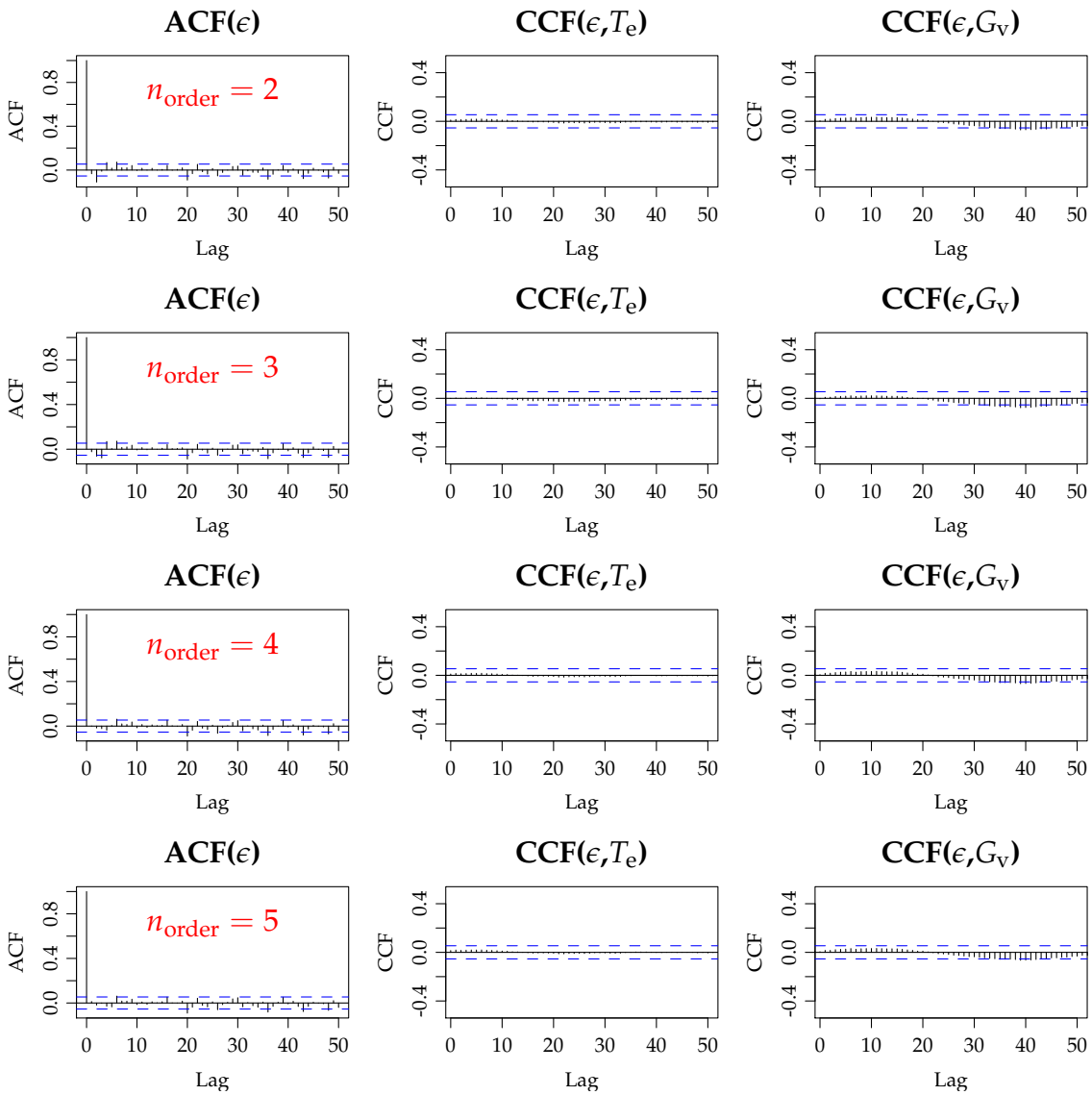


Figure 4.3: ARMAX model selection for $n_{\text{order}}$ 2, 3, 4 and 5 for 10 minutes values. The ACF of the residuals and the CCF from the residuals to the external temperature and the vertical global radiation.

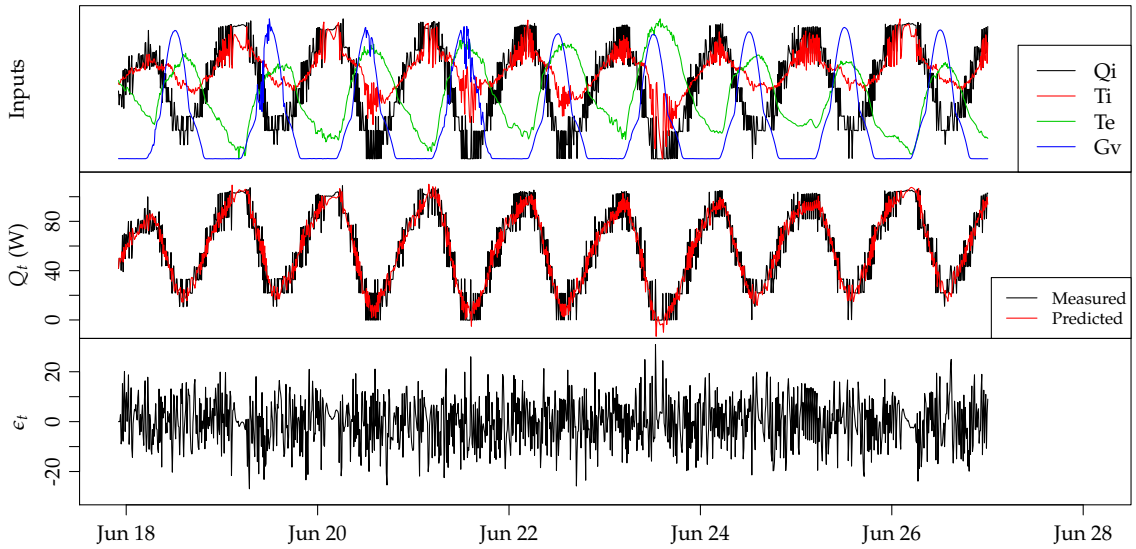


Figure 4.4: Validation of residuals for ARMAX model of $n_{\text{order}} = 4$ for 10 minutes values. The inputs are plotted in the upper plot, the measured and predict heat load in the middle, and the residuals in the lower plot.

## 4.2 Results

In this section the results from fitting ARMAX models for different sampling periods, using the proposed model selection procedure is presented. The estimated $UA$ and $gA$ values with 95% confidence bands are shown. First the results from fitting with the order of the $B_i$ polynomials set to $n_{\text{order}} - 1$, as for the ARX models, are plotted in Figure 4.5. It seems that there is a higher dependency on the sampling period, especially for the $UA$-value, compared to the results shown in Figure 4.6 where the order of the $B_i$ polynomials were always zero, therefore the latter is preferred and used when the results are compared between the different types of models.

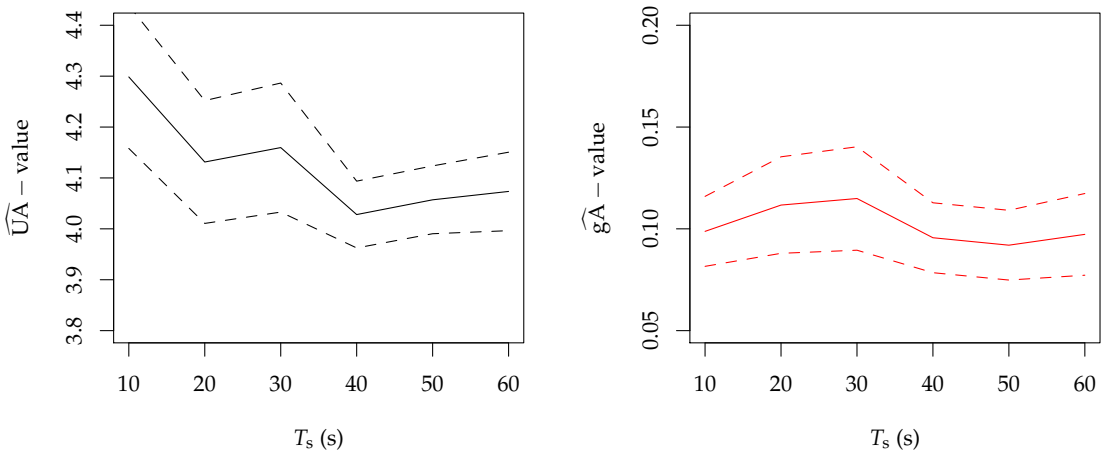


Figure 4.5: $UA$ and $gA$ estimates from ARMAX models for different sampling periods using thean order of the $B_i$ polynomials set to $n_{\text{order}} - 1$.

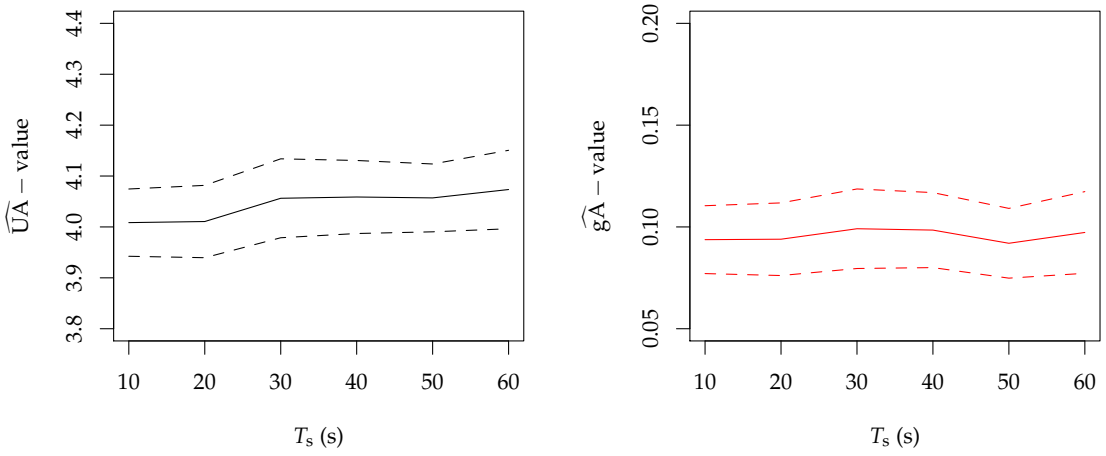


Figure 4.6: $UA$ and $gA$ estimates from ARMAX models for different sampling periods using the an order of the $B_i$ polynomials set to 0.

# Chapter 5

# Grey-box models

In this chapter the heat dynamics of the test box is modelled using grey-box models. The focus is on model selection and validation as well as estimation of the $UA$ and the $gA$ value of the test box. The data from CE4 Series 5 is used in which the heating was controlled with a ROLBS signal. A model is identified using a forward selection approach, where first a very simple model is fitted, which is then stepwise extended until a model validation shows that the assumption of white noise residuals is fulfilled. In each step only a single extension is presented, however several different extensions was examined in each step during the identification. In each step the loglikelihood is considered, it must increase significantly. The model evaluation for the selected model in each step is carried out by plotting the the auto-correlation function (ACF) and the cumulated periodogram (CP) of the standardized (one-step ahead) residuals, together with time series plots of them and the inputs. The stadardized residuals are

$$e_k^{\text{std}} = \frac{e_k}{\sigma_k} \tag{5.1}$$

where $\sigma_k^2$ is the estimated variance of the residuals. In the remaining of the report ”residuals” is used instead of the ”standized residuals” to simplify the text. The models are fitted to the data using CTSM-R, see Kristensen et al. (2004) and [1].

Using a sample period of 30 minutes was found as most appropriate in order to remove complex dynamical effects occuring after a switch in the heating signal.

## 5.1 Grey-box model for 30 minutes values

First the simplest feasible model is fitted. This model is denoted with $Model_{\text{Ti1}}$. It has a single state and system equation

$$dT_{\text{i}} = \left( \frac{1}{R_{\text{ie}} C_{\text{i}}} (T_{\text{e}} - T_{\text{i}}) + \frac{gA}{C_{\text{i}}} \Phi_{\text{s}} + \frac{1}{C_{\text{i}}} \Phi_{\text{h}} \right) dt + \sigma_{\text{i}} d\omega_{\text{i}} \tag{5.2}$$

and the measurement equation

$$Y_k = T_{\text{i},k} + \epsilon_k \tag{5.3}$$

[1] ctsm.info

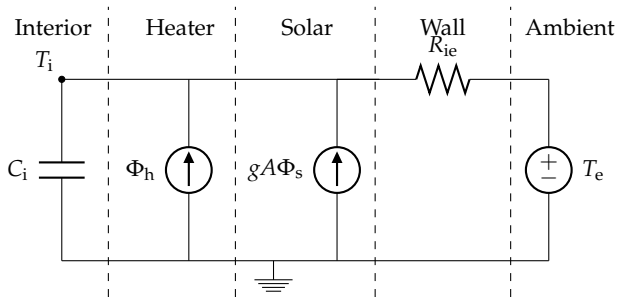


Figure 5.1: RC-network of the most simple $Model_{Ti1}$ and $Model_{Ti}$.

The measurement equation is the same for all the grey-box models fitted. See for example (Madsen and Holst, 1995) and Bacher and Madsen (2011) for more details on the formulation of the grey-box models. $\Phi_s$ is the vertical south faced global radiation and $Ph$ is the heating. This model can be represented with the RC-diagram in Figure 5.1. The fit is evaluated considering the plots in Figure 5.2. From the ACF the residuals seems to be white noise, however checking the time series plot of the residuals clearly the residuals are not white noise. There are two different regimes in the process generating the residuals: when the periods in the heating signal are short then the level of the residuals is higher than when the switching periods are long, hence the variance is not constant, hence the error process is not stationary. Secondly, when the residual level is low, it can be seen that the residuals are clearly correlated. This is a very clear example showing that only checking the ACF and CP of the residuals are not sufficient for the model evaluation, since a non white noise series can have an ACF indicating white noise, and therefore time series plots of the residuals also needs to be considered in the evaluation. To take care of the two different levels of the residuals two levels of system noise is included in the model. A signal is generated based on the switching points $t_i^{\mathrm{sw}}$ of the heating signal

$$\rho_t^{\mathrm{r}} = \begin{cases} 1 \ for \ \ t \in \ [t_i^{\mathrm{sw}},\, t_i^{\mathrm{sw}} - 0.5\mathrm{h} + 2.5\mathrm{h}]_{\{i \in \mathbb{Z}^+\}} \\ 0 \ for \ \ t \notin \ [t_i^{\mathrm{sw}},\, t_i^{\mathrm{sw}} - 0.5\mathrm{h} + 2.5\mathrm{h}]_{\{i \in \mathbb{Z}^+\}} \end{cases} \tag{5.4}$$

hence 0.5 hour and until 2.5 hours after a switch the signal is 1 else it is 0. This signal is then used in $Model_{Ti}$ to switch between two levels of system noise

$$dT_i = \left( \frac{1}{R_{ie}C_i}(T_e - T_i) + \frac{gA}{C_i}\Phi_s + \frac{1}{C_i}\Phi_h \right) dt + (1 + \rho_r\sigma_r)\sigma_i d\omega_i \tag{5.5}$$

Hence $\sigma_i$ will be the low system noise level and $\sigma_i + \sigma_r$ is the high level. The RC-diagram in Figure 5.1 also represents this model.

The $Model_{Ti}$ is fitted to data and the evaluation plots are shown in Figure 5.3. First it is noted that the introduction of two system noise levels results in much more stationary residuals series in the sense of a time independent variance. The ACF and CP are still indicating almost white noise, however the residuals time series plots again clearly reveal non white noise residuals. Furthermore, in the plot of the measured and one-step predicted indoor temperature a "one-step lag" is observed, especially evident after an on/off switch in the heating. This strongly indicates that the model is very poor in predicting the fast dynamics. Hence the model needs to

be extended with an additional state in order to better describe the fast dynamics. A state variable representing the wall temperature is introduced in $Model_{\text{TiTw}}$

$$dT_{\text{i}} = \left( \frac{1}{R_{\text{ia}}C_{\text{i}}}(T_{\text{w}} - T_{\text{i}}) + \frac{gA}{C_{\text{i}}}\Phi_{\text{s}} + \frac{1}{C_{\text{i}}}\Phi_{\text{h}} \right) dt + (1 + \rho_{\text{r}}\sigma_{\text{r}})\sigma_{\text{i}} d\omega_{\text{i}} \tag{5.6}$$

$$dT_{\text{w}} = \left( \frac{1}{R_{\text{iw}}C_{\text{w}}}(T_{\text{i}} - T_{\text{w}}) + \frac{1}{R_{\text{we}}C_{\text{w}}}(T_{\text{e}} - T_{\text{w}}) \right) dt + (1 + \rho_{\text{r}}\sigma_{\text{r}})\sigma_{\text{e}} d\omega_{\text{e}} \tag{5.7}$$

The RC-diagram representing the model is shown in Figure 5.4. The model is fitted to the 30 minutes values and the evaluation plots are shown in Figure 5.5. The ACF of the residuals clearly indicates that the residuals are not white noise, this is even much more than for the previous model, however the level of the non-standardized residuals have decreased and the log-likelihood has increased considerably, hence it is evident that the model is more suitable than the single-state $Model_{\text{Ti}}$.

The next extension is created by adding a part in which the solar radiation is absorbed in the wall state in $Model_{\text{TiTw.GinTw}}$

$$dT_{\text{i}} = \left( \frac{1}{R_{\text{ia}}C_{\text{i}}}(T_{\text{w}} - T_{\text{i}}) + \frac{p\,gA}{C_{\text{i}}}\Phi_{\text{s}} + \frac{1}{C_{\text{i}}}\Phi_{\text{h}} \right) dt + (1 + \rho_{\text{r}}\sigma_{\text{r}})\sigma_{\text{i}} d\omega_{\text{i}} \tag{5.8}$$

$$dT_{\text{w}} = \left( \frac{1}{R_{\text{iw}}C_{\text{w}}}(T_{\text{i}} - T_{\text{w}}) + \frac{1}{R_{\text{we}}C_{\text{w}}}(T_{\text{e}} - T_{\text{w}}) + \frac{(1-p)gA}{C_{\text{i}}}\Phi_{\text{s}} \right) dt + (1 + \rho_{\text{r}}\sigma_{\text{r}})\sigma_{\text{e}} d\omega_{\text{e}} \tag{5.9}$$

hence the parameter $p$ determines the share entering the interior (indoor air) and the remaining $(1 - p)$ is absorbed in the wall. In this formulation there is, for the part absorbed in the wall, no distinction whether it enters into the wall from the inside or from the outside surface. The RC-diagram in Figure 5.6 represents the model. The model is fitted and the model evaluation plots are shown in Figure 5.7. It is seen that the level of the residuals has decreased and the log-likelihood has increased compared to the previous model.

The next extension is carried out by adding one more state in the wall and let the solar radiation enter into the inner state of the wall. The $Model_{\text{TiTw2.GinTw}}$ is fitted and the evaluation plots are shown in Figure 5.8. The ACF and CP indicates that the residuals are close to white noise properties and no clear patterns can seen in the residuals series plot. No real significant improvement is found and a likelihood-ratio test (Bacher and Madsen, 2011) between $Model_{\text{TiTw.GinTw}}$ and $Model_{\text{TiTw2.GinTw}}$ has a p-value very close to one, hence the improvement of adding a second state is not significant. Therefore $Model_{\text{TiTw.GinTw}}$ is selected for assessing the performance of the box.

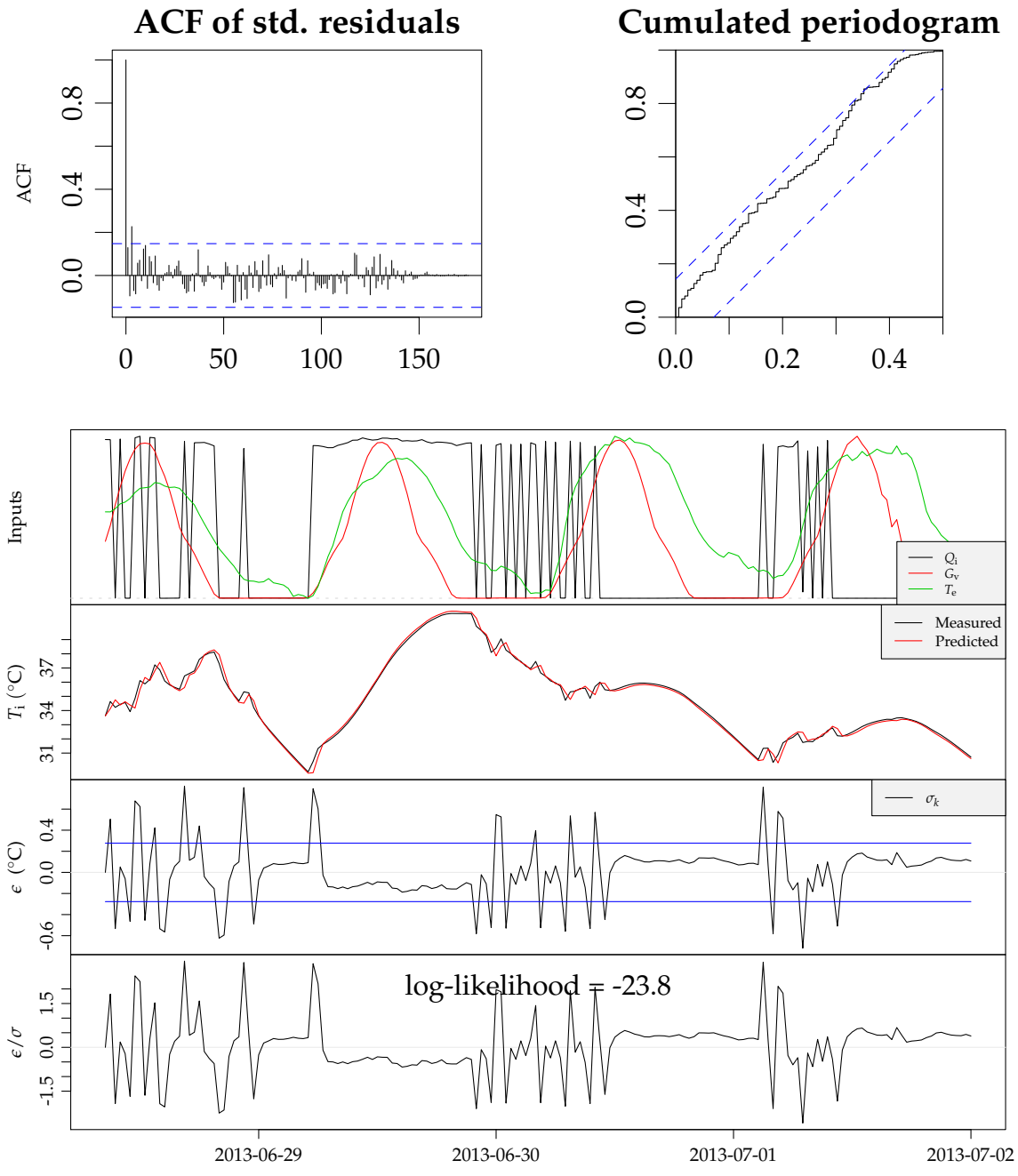


Figure 5.2: Residuals for $Model_{\text{Ti1}}$

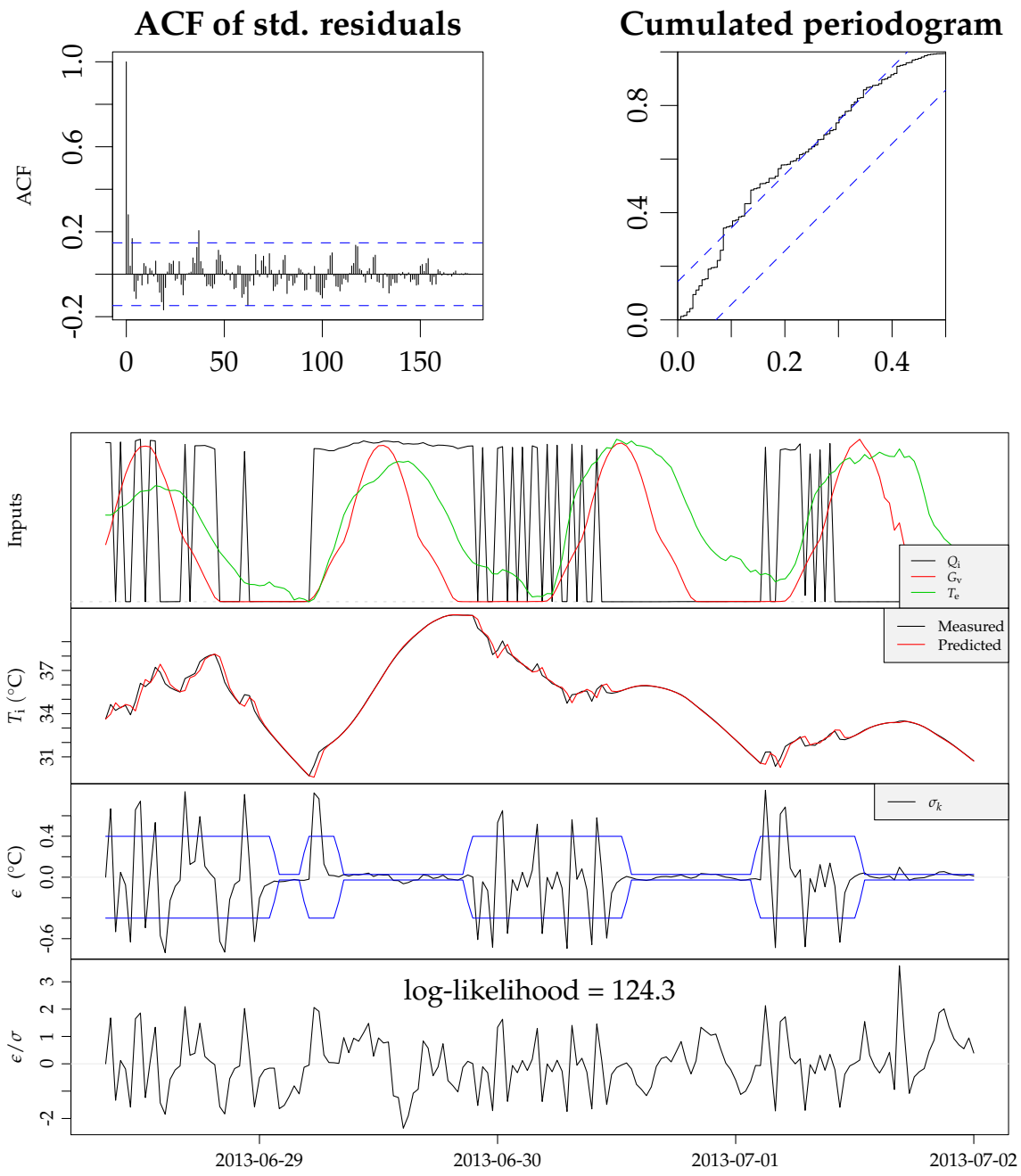


Figure 5.3: Evaluation plots for $Model_{\mathrm{Ti}}$

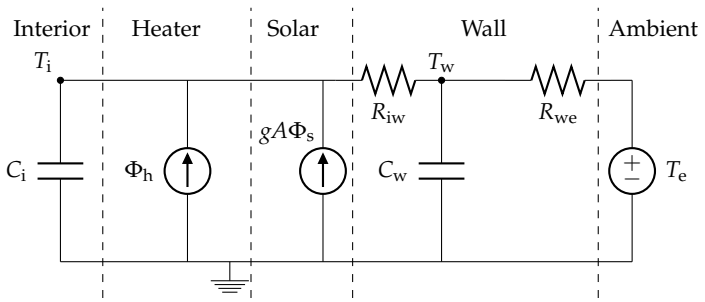


Figure 5.4: RC-network of the $Model_{\mathrm{TiTw}}$.

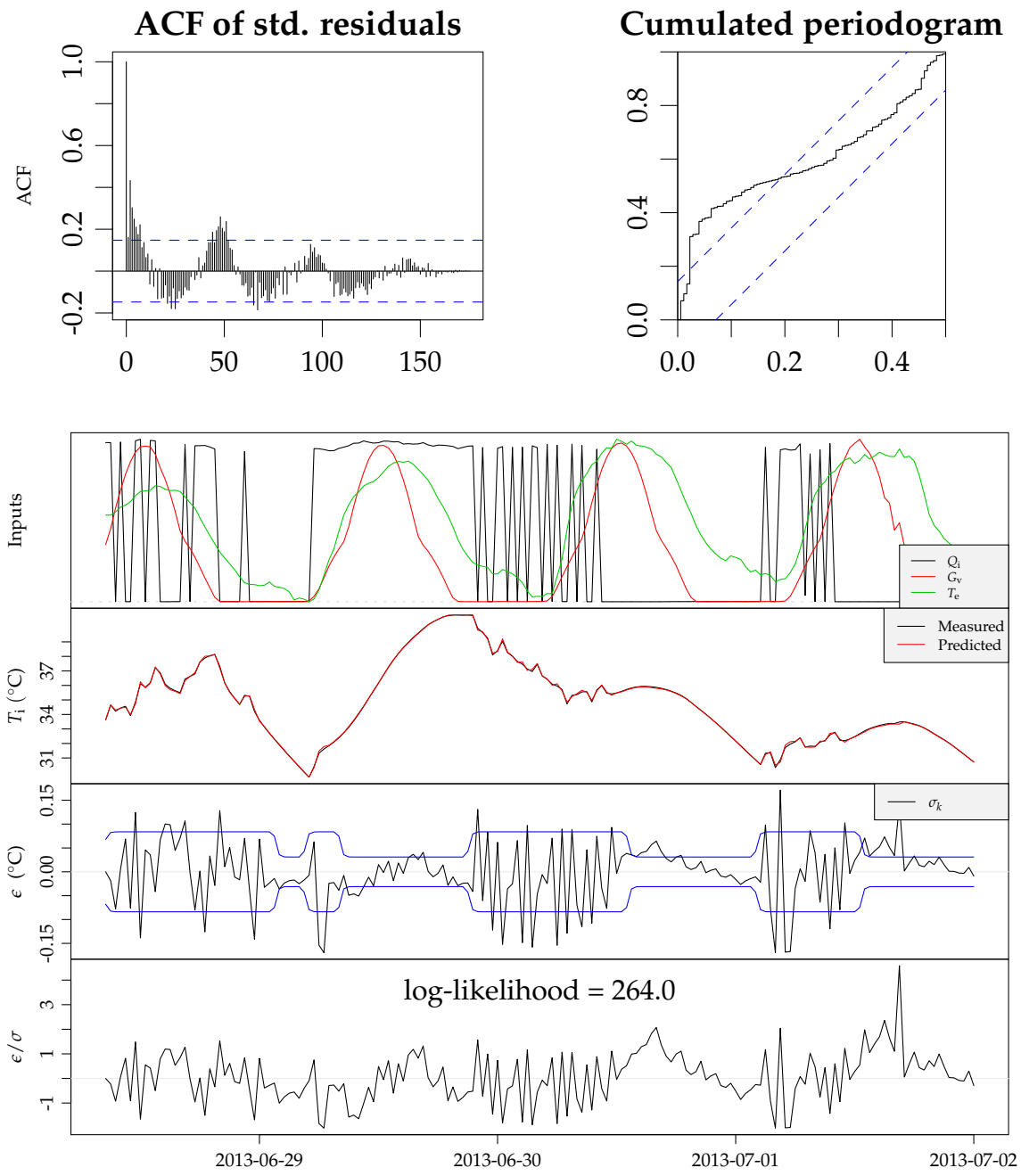


Figure 5.5: Evaluation plots for $Model_{\text{TiTw}}$

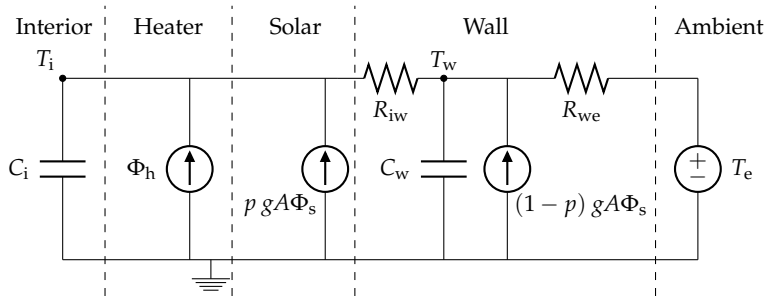


Figure 5.6: RC-network of the $Model_{\text{TiTw.GinTw}}$.

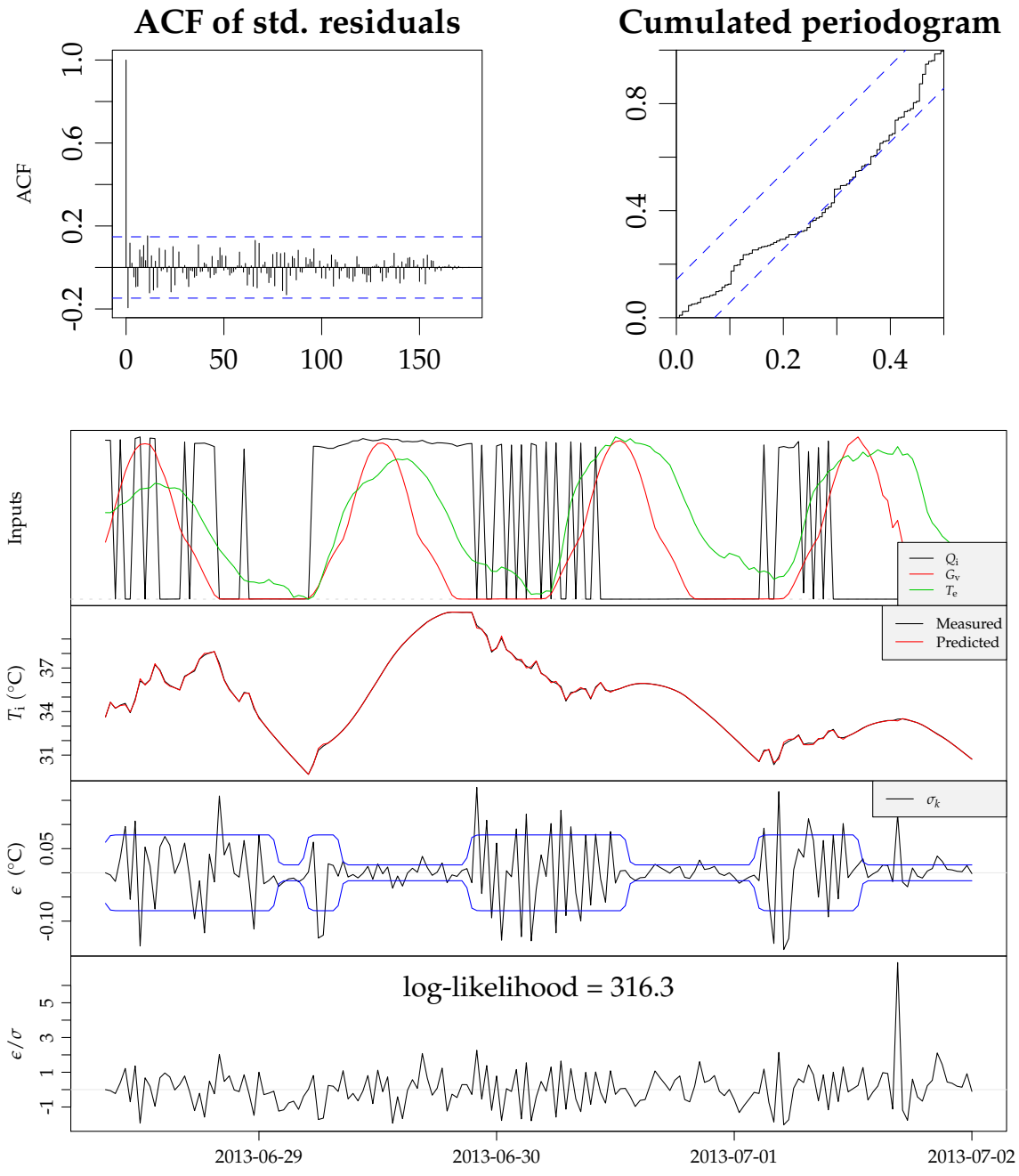


Figure 5.7: Evaluation plots for $Model_{\text{TiTw.GinTw}}$

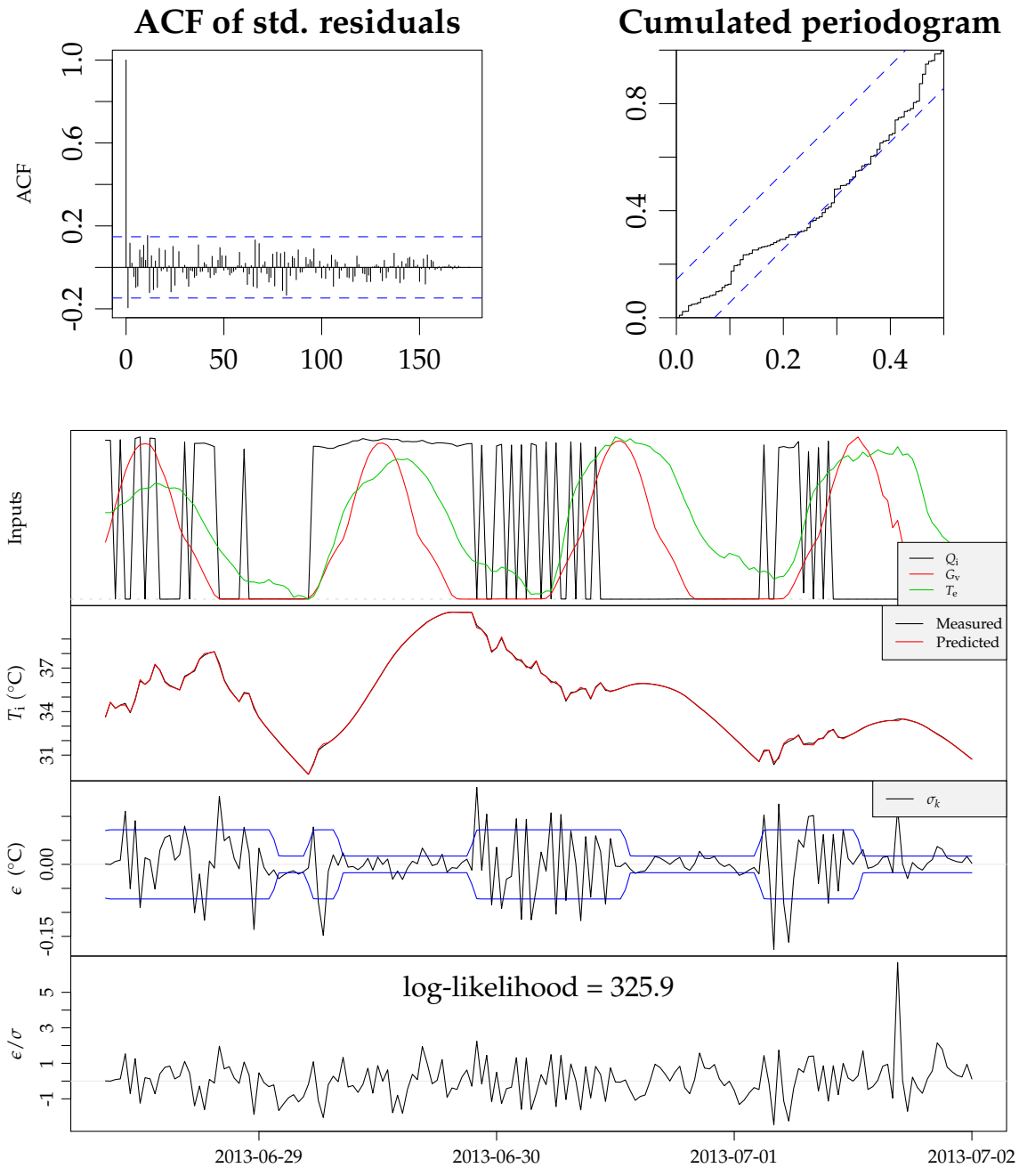


Figure 5.8: Evaluation plots for $Model_{\text{TiTw2.GinTw}}$

### 5.1.1 Results

In this section the estimated parameters with the selected model is evaluated. The estimated parameters are listed in Table 5.1. Firstly it is noted that all parameters

| | Estimate | Std.Error | p-value | unit |
|---|---|---|---|---|
| $\hat{T}_0^{\mathrm{i}}$ | 3.4E+01 | 6.7E-02 | 0.0E+00 | °C |
| $\hat{T}_0^{\mathrm{w}}$ | 3.2E+01 | 2.3E-01 | 0.0E+00 | °C |
| $\hat{C}_{\mathrm{i}}$ | 5.7E+04 | 9.1E+02 | 0.0E+00 | J/°C |
| $\hat{C}_{\mathrm{w}}$ | 3.1E+05 | 8.9E+03 | 0.0E+00 | J/°C |
| $\hat{R}_{\mathrm{iw}}$ | 4.1E-02 | 1.4E-03 | 0.0E+00 | °C/W |
| $\hat{R}_{\mathrm{we}}$ | 2.1E-01 | 5.2E-03 | 0.0E+00 | °C/W |
| $\widehat{gA}$ | 1.4E-01 | 7.3E-03 | 0.0E+00 | $\mathrm{m}^2$ |
| $\hat{p}$ | 2.9E-01 | 3.4E-02 | 1.4E-14 | |
| $\hat{\rho}_{\mathrm{r}}$ | 4.4E+00 | 7.0E-01 | 3.6E-09 | |
| $\hat{\sigma}_{\mathrm{i}}$ | 1.9E-08 | | | |
| $\hat{\sigma}_{\mathrm{w}}$ | 8.9E-04 | | | |
| $\hat{\sigma}$ | 1.0E-05 | | | |

Table 5.1: Estimated parameters with standard deviance and p-value of t-test for significance.

are significant indicating that the model is not over-fitted. The heat capacities are somewhat in the range and the thermal resistances indicate that the wall temperature state is located towards the inner of the walls. The $p$ estimate indicates that most of the solar radiation is absorbed in the wall state and less in the interior state.

The estimated $UA$-value and $gA$-value for the box is calculated with their 95% confidence bands. The $UA$-value is

$$\widehat{UA} = \frac{1}{\hat{R}_{\mathrm{iw}} + \hat{R}_{\mathrm{we}}} = 3.96 \pm 0.14 \tag{5.10}$$

and the $gA$ value is

$$\widehat{gA} = 0.145 \pm 0.013 \tag{5.11}$$

### 5.1.2 Discussion and further work

The test sequence should be reconsidered in order to be more suitable for the current performance assessment. The level of the residuals after a switch in the heating signal is clearly much higher than for the periods where the they either on or off. This is well handled by having two levels of residuals, however as the residuals are close to white noise at this sampling period, it seems not feasible to improve the model to describe this. This results in a higher signal to noise ratio (s/n-ratio) which implies that the uncertainty of the performance estimates increase and that effects cannot be seen in the data. Alternatively a solution could be to use of a lower re-sampling period and more detailed modelling of the fast dynamical effects, however, since the current performance characterization do not consider dynamics its measures ($UA$ and $gA$), but instead only the stationary performance, it would be much more relevant to design the experiment such that there are less of

the fast dynamics in the data. This can be achieved both by using less fast switching in the heating signal, or smooth the transitions, either by linear interpolation between the on/off states or low-pass filtering the heating signal before carrying out the experiments.

Further improvements could be achieved by a more detailed description of the effect of solar radiation in the model, since now only the vertical radiation is used as input and the $gA$-value is thus assumed constant over the day. It can be carried out by either a more detailed prior calculation of the solar radiation entering the outer surface or by a non-parametric approach as discussed in Section ??. However it might not be possible gain more information on the effect of solar radiation with the current s/n-ratio.

# Chapter 6

# Enhanced description of solar radiation effects

In this section an enhanced description of the solar radiation effects is presented. The focus is on including a semi-parametric description of the varying effect of solar radiation depending on the position of the sun. Clearly, the current assumption of a constant $gA$-value is not appropriate when modelling with a time-resolution below daily values. The properties of the surfaces of the box will change the absorption of solar radiation as a function of the position of the sun. This effect can be modelled in details by using prior physical knowledge, however in the present work a semi-parametric approach is suggested, which have some advantages and disadvantages compared to a more physical based approach. The main advantage is that no assumptions and prior knowledge of the building are needed, rather this can be learned based on the results from the suggested approach. The disadvantage of using less prior information is that less details of the actual physical processes occuring can be inferred on. The models used are ARX models, in later studies the semi-parametric approach should also be applied for grey-box models. The data used are 30 minutes values from CE4 Series 4 and for one of the models the similar data from CE3 is used.

The estimated $UA$ values for all models fitted in this section are summarized in Table 6.1.

## 6.1 Splined solar radiation input

In this section the use of base splines for modelling the $gA$-value as a function of the sun azimuth angle is presented. The base splines are calculated using the `R` package `splines`, to read more on base splines see the documentation of the `splines` package or (De Boor et al., 1993). The splines are constructed by taking the range from minimum to maximum sun azimuth angle where the sun elevation is positive, and over this range calculate second order base splines using on two evenly distributed knots. This results in five base splines shown in Figure 6.1. By multiplying the base splines to a solar radiation series

$$S_{i,t}^{G_x} = B_{i,t} G_t^x \tag{6.1}$$

and using this as input to an ARX model, the solar absorption coefficient ($gA$-value) can vary as a smooth function of the sun azimuth angle. Note that the inter-

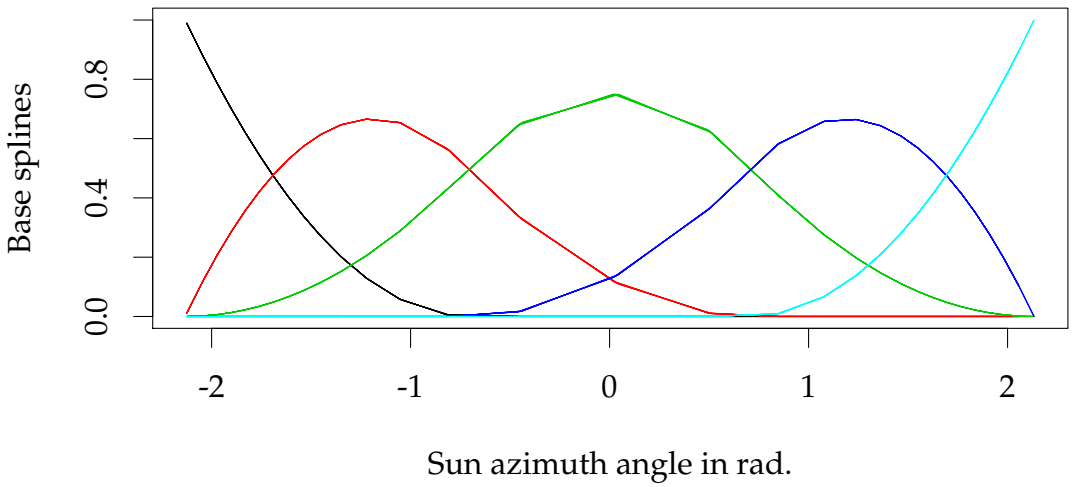


Figure 6.1: Base splines used.

pretation of the $gA$-value estimates will be completely different, simply depending on which solar radiation measurements are used. The following three are used:

- Spline the south faced vertical global radiation $G_{\text{vs}}$
- Spline the beam radiation $G_{\text{b}}$ and use also the diffuse radiation as input
- Spline the horizontal global radiation $G$

In the first model in which the base splines are used is with the south faced global radiation to form the ARX Spline $G_{\text{vs}}$ model

$$A(q)Q_t = b_{1,0}T_t^{\text{i}} + B_2(q)T_t^{\text{a}} + b_{\text{sp1}}\, S_{1,t}^{G_{\text{vs}}} + \cdots + b_{\text{sp5}}\, S_{5,t}^{G_{\text{vs}}} + \epsilon_t \tag{6.2}$$

where

$$A(q) = 1 + a_1 q^{-1} + a_2 q^{-2} + \cdots + a_{n_{\text{order}}} q^{-n_{\text{order}}} \tag{6.3}$$

$$B_i(q) = b_{i,0} + b_{i,1} q^{-1} + b_{i,2} q^{-2} + \cdots + b_{i,n_{\text{order}}-1} q^{-(n_{\text{order}}-1)} \tag{6.4}$$

The model order $n_{\text{order}}$ is found to be 4 to achieve white noise residuals, as seen from the plots in Figure 6.2. The same model order was found independent of which splined solar input: vertical north or south, horizontal or beam, was used, the ACF plots are quite similar and are leaved out for simplicity.
The estimated $gA$ for vertical south faced global radiation as a function of the sun azimuth is shown in Figure 6.3. Both the CE3 and CE4 data is used and the results for each are shown. For CE4 the $gA$ function increase in the morning and afternoon. This makes sense since on the south surface only diffuse radiation is measured, which is much less than the actual radiation entering the other surfaces of the box. In the middle of the day the level of the $gA$ function is between 0.1 to 0.12, which is close to the constant $gA$ estimates found previous with $G_{\text{vs}}$, and since this is the time where most solar radiation is entering the box (through the window) this level is found very reasonable. The similarly estimated $gA$ function

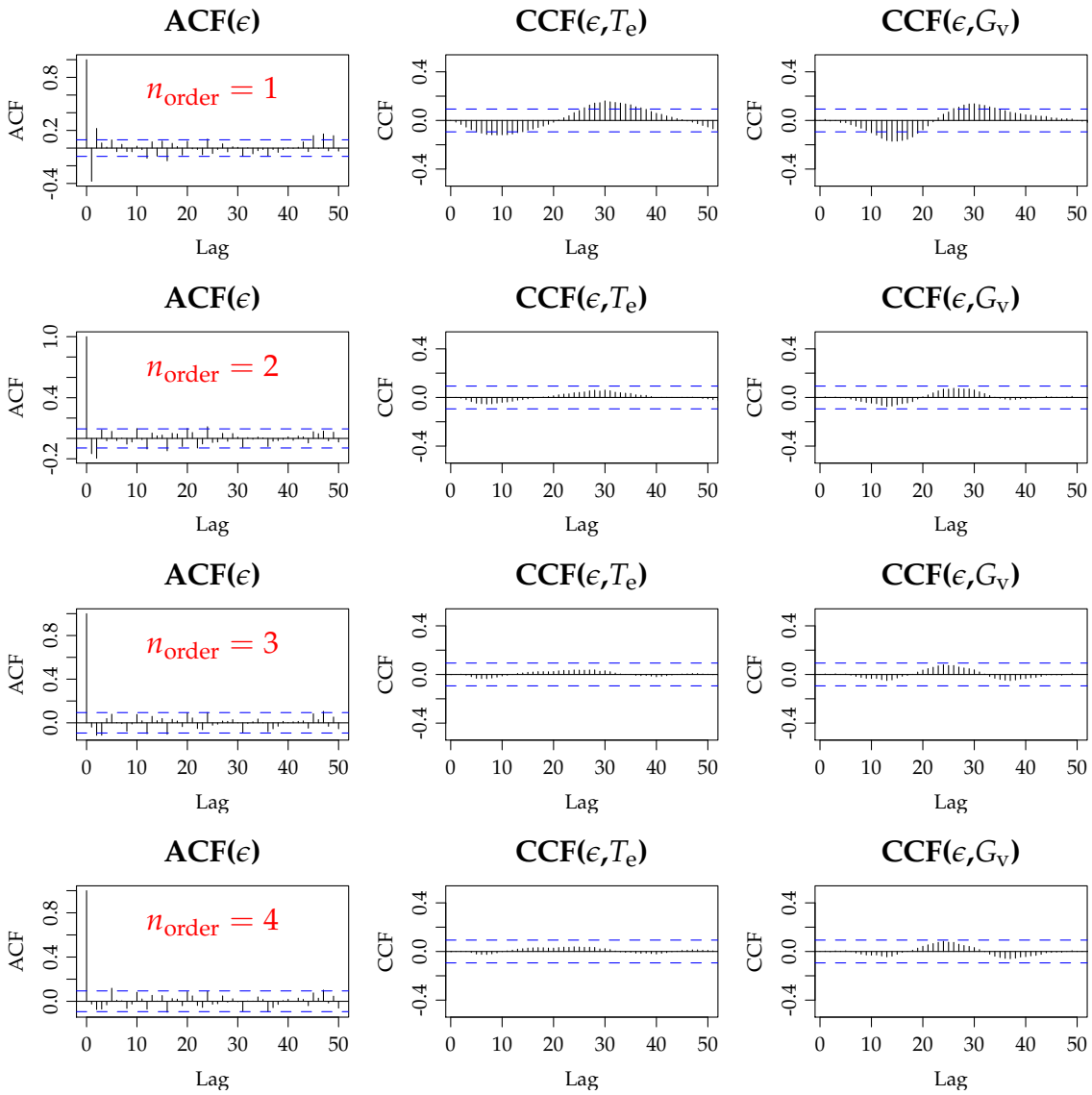


Figure 6.2: Model selection for $n_{\text{order}}$ of 1 to 4 for 30 minutes values for the ARX with splined vertical south faced global radiation input. The ACF of the residuals and the CCF from the residuals to the external temperature and the vertical global radiation.

for the CE3 has approximately the same level in the middle of the day, however in the morning it has oppositely a decrease towards zero. This could be explained by the fact that the level of solar radiation is low for the CE3 data and the sun elevation is low, however the cause of the decreasing behavior is not really clear.

The second fitted spline model is using the base splines with the beam radiation and also including the horizontal diffuse radiation in the model

$$A(q)Q_t = b_{1,0}T_t^{\text{i}} + B_2(q)T_t^{\text{a}} + B_3(q)G_t^{\text{dif}} + b_{\text{sp1}}\,S_{1,t}^{G_{\text{b}}} + \cdots + b_{\text{sp5}}\,S_{5,t}^{G_{\text{b}}} + \epsilon_t \qquad (6.5)$$

The estimated $gA$ function which plotted in Figure 6.4 for CE4 only, since the beam radiation was not measured in the CE3 experiments. The horizontal beam radiation could be calculated for CE3 and projected to the plane normal to the solar beam radiation, however this is left for further work. The estimated $gA$ function for the beam radiation is lower in the morning, which is because there are no win-

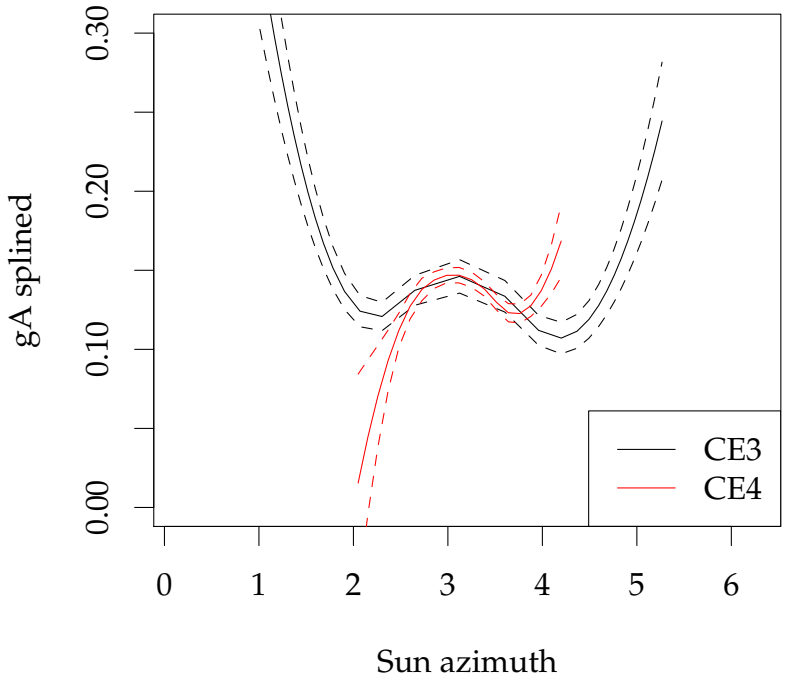


Figure 6.3: $gA$ varying as a function of the sun azimuth based on south faced vertical solar radiation $G_{vs}$. The dashed lines marks the 95% confidence bands.

dows in the surfaces of the box which is hit by the beam solar radiation in the morning and evening hours. The level around 0.04 which is reached in the middle of the day, when the sun is from south, makes sense compared to the level of 0.11 estimated for the vertical south faced radiation, since the angle of incidence of the beam radiation on the south faced surface with window is high (i.e. the sun elevation is high), thus less of the measured beam radiation is absorbed compared to the vertical radiation.

Finally, the horizontal global radiation is used with splines for both CE3 and CE4. The estimated $gA$ as a function of the sun azimuth is shown in Figure 6.5 for both CE3 and CE4. Clearly, this does not give comparable functions, since the sun elevation is very different for the two experiments, rather a projection from horizontal to the plane normal to the beams should be carried, this should be studied in further work.

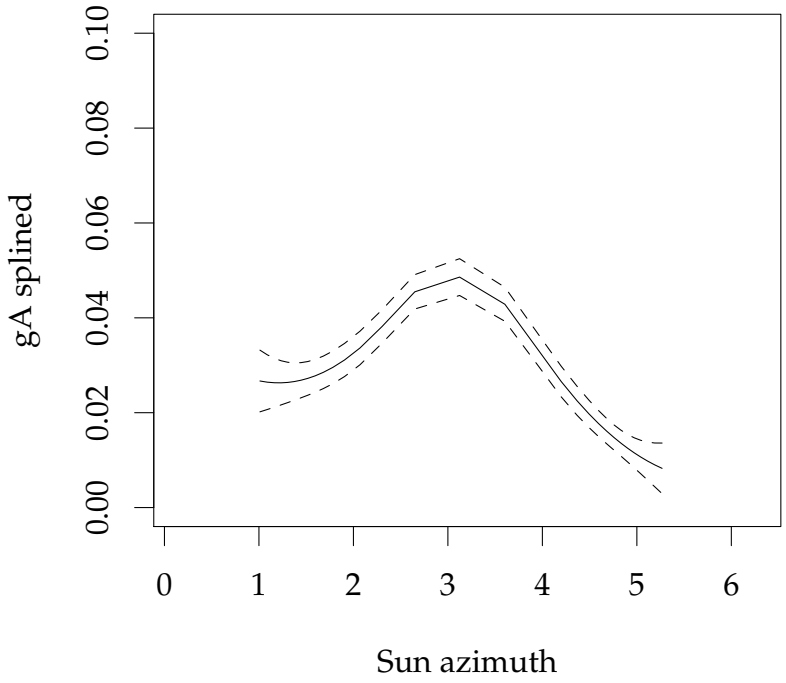


Figure 6.4: Use diffuse as input together with beam radiation for $gA$ value varying as a function of the sun azimuth. The dashed lines marks the 95% confidence bands.

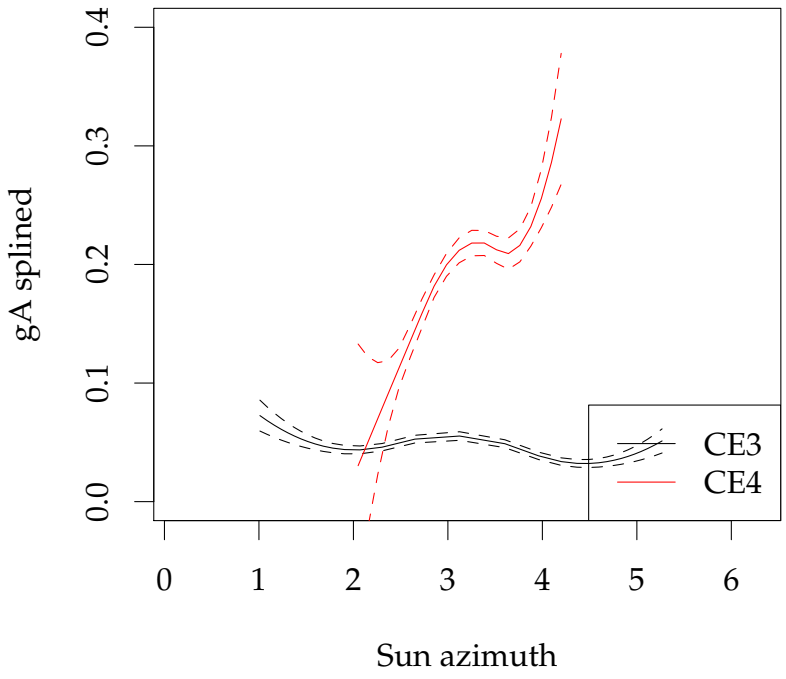


Figure 6.5: The $gA$ as a function of sun azimuth angle using horizontal global radiation with splines. The dashed lines marks the 95% confidence bands.

### 6.1.1 *UA*-value estimates

The estimated *UA* values using the models with the splined solar models are listed in Table 6.1. Very interestingly the *UA*-value increases slightly for CE4 compared to the *UA*-values for the ARX models presented in Table 3.1 (page 17), however it doesn't increase for CE3. This is discussed further in the following section.

| | $G_{vn}$: $\widehat{UA}$ | $1.97\hat{\sigma}_{UA}$ | $G_{vs}$: $\widehat{UA}$ | $1.97\hat{\sigma}_{UA}$ | $G_b$: $\widehat{UA}$ | $1.97\hat{\sigma}_{UA}$ | $G$: $\widehat{UA}$ | $1.97\hat{\sigma}_{UA}$ |
|---|---|---|---|---|---|---|---|---|
| CE3 | | | 3.97 | 0.02 | | | 3.99 | 0.02 |
| CE4 | 4.27 | 0.05 | 4.29 | 0.06 | 4.29 | 0.05 | 4.26 | 0.06 |

Table 6.1: *UA*-values estimated with the splined solar models for both CE3 and CE4, including 95% confidence bands.

### 6.1.2 Comparison to ARX models

In this section a rough comparison is carried between the ARX model identified in Section 3.2.1 and the ARX spline model identified above in this section (Section 6.1). Both using the south faced global radiation ($G_{vs}$). In Figure 6.6 the residuals for both models are plotted versus the time of day. A slight pattern is seen, which is more pronounced for the ARX model compared to the ARX spline model, hence is seems like the splined gA function does decrease the bias and take into account better the dependence of the position of the sun. Finally, an F-test is carried out for comparison of the two fits to test if the ARX spline model is more suitable than the ARX model. The residual sum of squares (RSS) for the ARX model is 8943 and for the ARX spline model 8280, which does seem as a significant decrease. An F-test requires that the smaller model (the ARX model) is a sub model of the larger model (the ARX spline model). This is not entirely the case, since two more lags are included for solar input in the ARX model ($b_{3,1}$ and $b_{3,2}$, see Equation (6.3)), which are no the ARX spline model, they are not included when the solar spline input is used. However, this does not influence the outcome of the test, since subtracting two from the number of coefficients for the ARX model gives a p-value of the test at 0.000012, which indicates a very significant improvement for the ARX splined model over the ARX model.

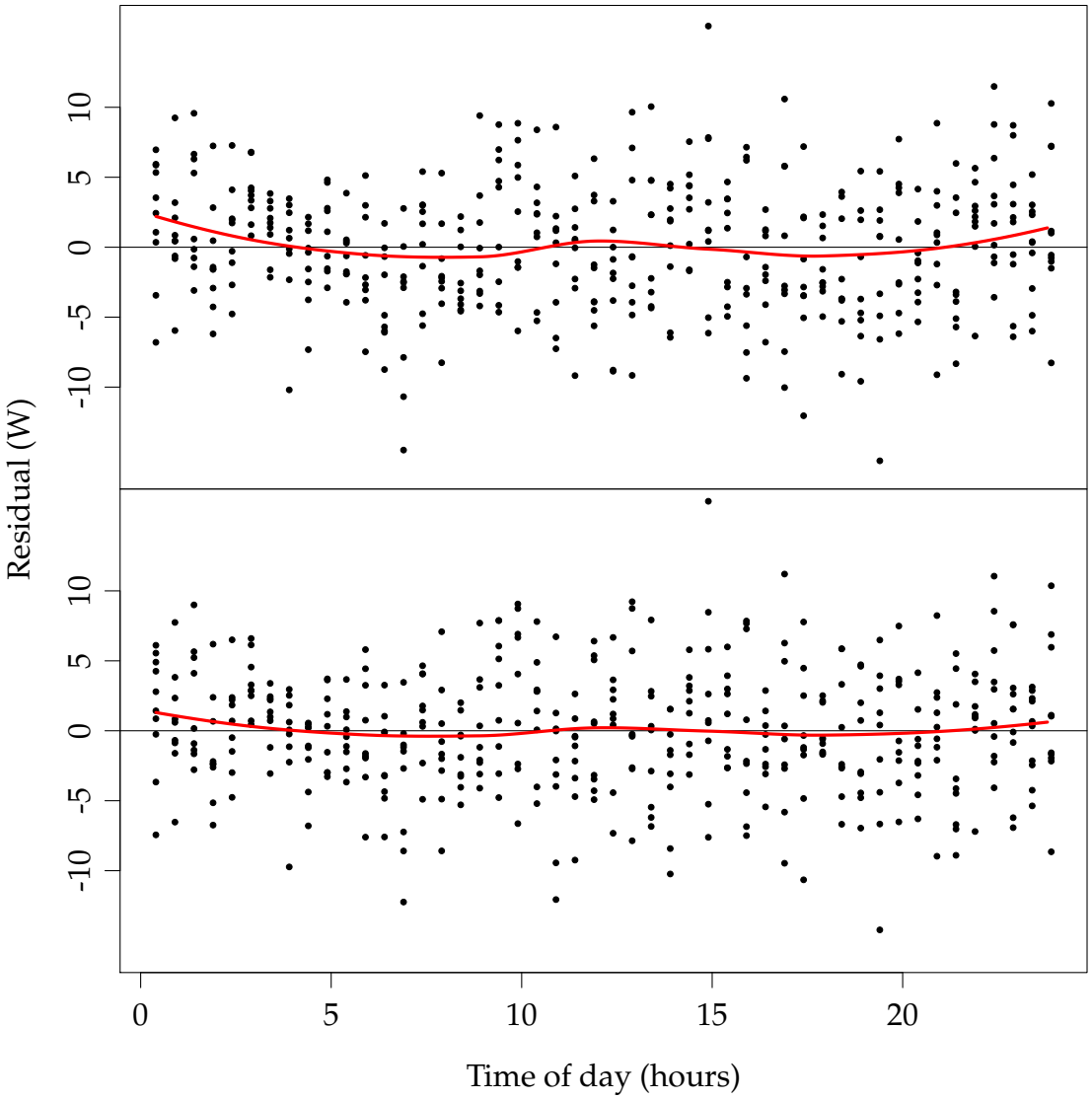


Figure 6.6: The residuals versus the time of day, with a local regression line calculated with the R R Core Team (2013) function loess() with default values. The upper plot is for the ARX model and the lower plot is for the ARX spline model.

## 6.2 Discussion

In order to compare $gA$ as a function of solar azimuth for different climate the type of observed solar radiation needs to be carefully considered. Furthermore, the characterization is actually a function of both sun azimuth and elevation, hence a surface in these two dimensions could be fitted, but for the current data sets observed under different climate conditions only the function within limited ranges can be estimates. Preferably the beam radiation should be used, however this is more complicated to measure compared to the horizontal radiation. In further works the global horizontal radiation should splitted using for example a scheme suggested by Ruiz-Arias et al. (2010) and projected to the plane normal to the direct solar radiation.

# Chapter 7

# Comparison of results from CE3 and CE4

In this section the estimated *UA* and *gA* values are compared for the models applied for both CE3 and CE4.

## 7.1 ARX and ARMAX models for CE3 and CE4

The ARX models presented in Section 3 are applied for both CE3 and CE4 following model selection procedure for a range of sample periods. In Figure 7.1 the estimated *UA* and *gA* values with 95% confidence intervals are shown. It is

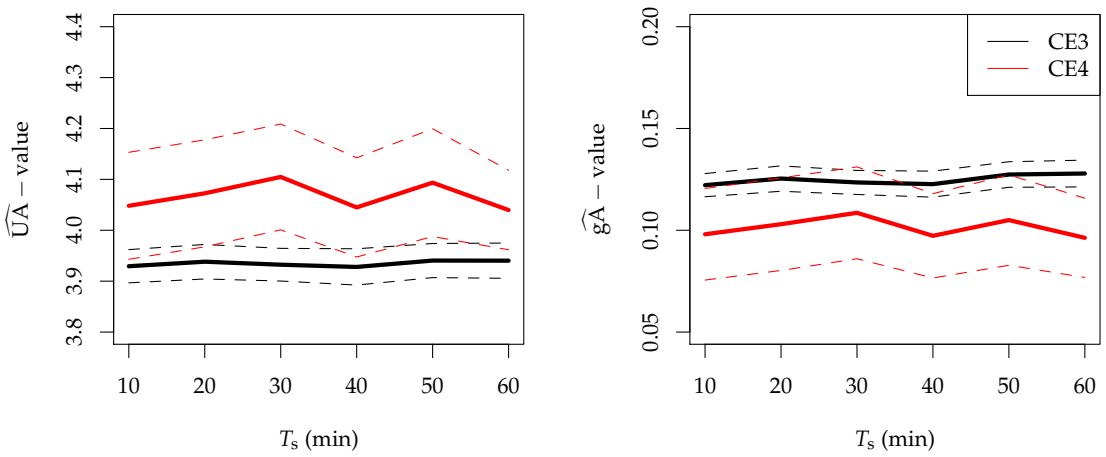


Figure 7.1: ARX both for CE3 and CE4 data. Estimates of the *UA*-value and *gA*-value found using the model selection procedure for 10, 20, 30, 40, 50 and 60 minutes values, together with the 95% confidence bounds.

seen that the *UA*-values are a bit lower for CE3 compared to CE4, and also with a lower uncertainty for CE3. There might be a physical explanaition for the lower *UA*-values, however the authors do not have knowlegde of this. From a statistical point of view the coefficients for the ambient temperature and the solar radiation might be more correlated in the CE4 data, since the level of solar radiation is high and with almost the same pattern every day. This correlation could also explain

the increased uncertainty for CE4 estimates. The $gA$-values decrease for CE4 compared to CE3, which can be explained by the different sun elevation patterns in the experiments having an influence on the angle of incidence, especially on the south facade. If this is the case, then practically the $gA$-value estimates cannot be compared directly. Again the uncertainty is clearly higher for CE4.

Similarly, the ARMAX models are fitted for CE3 and CE4. The $UA$ and $gA$ value estimates are shown in Figure 7.2. The estimates seems to be slightly more unstable than the estimates from the ARX models, however the $UA$-value estimates are more similar between CE3 and CE4, but still with higher values and uncertainties for CE4. The $gA$-values have a similar pattern as for the ARX models, it can be noted that the uncertainties are generally higher for CE3 compared to the ARX models.

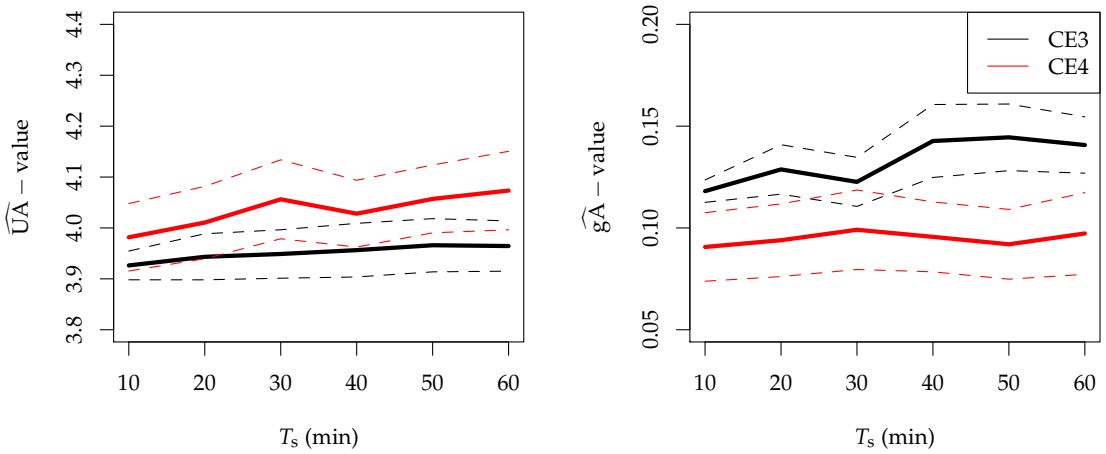


Figure 7.2: ARMAX both for CE3 and CE4 data. Estimates of the $UA$-value and $gA$-value found using the model selection procedure for 10, 20, 30, 40, 50 and 60 minutes values, together with the 95% confidence bounds.

## 7.2 Comparison of results from grey-box models for CE3 and CE4

The $Model_{\text{TiTw.GinTw}}$ is fitted to both CE4 Series 5 data and the similar data for CE3 (the ROLBS series). The ACF and CP for the model fitted to each series are shown in Figure 7.3. Clearly the ACF and CP indicate white noise residuals for CE3 and very close to white noise for CE4. The estimated $UA$ and $gA$ values are listed in Table 7.1. The $UA$ estimates are slightly lower for the CE3 and also the uncertainty is much lower, which is the same pattern as for the other models. Again the $gA$ value is estimated higher for CE3, which again can be explained by the difference in sun elevation between the two experiments.

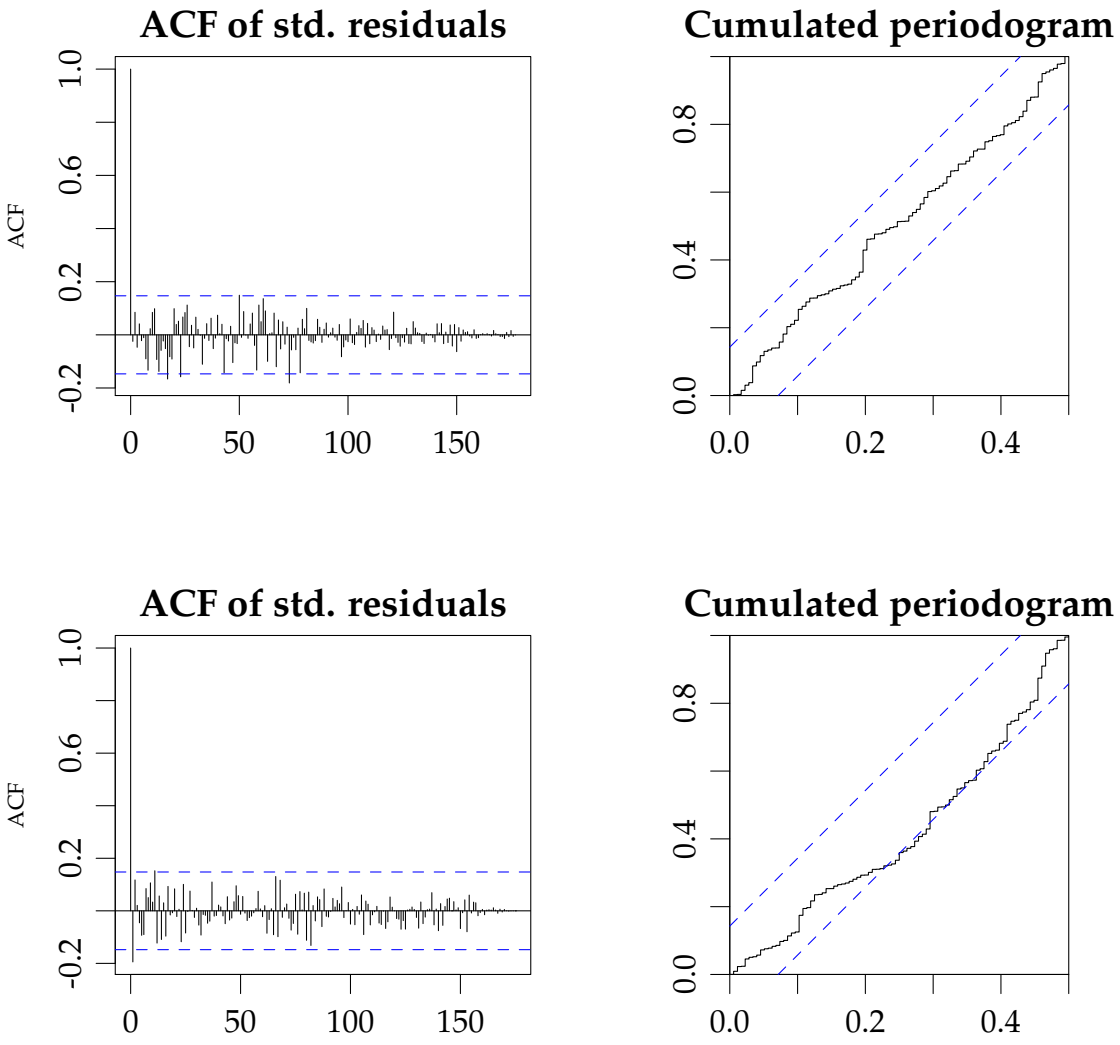


Figure 7.3: ACF and cumulated periodogram for the CE3 (upper) and CE4 (lower).

| $\widehat{\mathrm{UA}}$ | $\hat{\sigma}_{\mathrm{UA}}$ | $\widehat{\mathrm{gA}}$ | $\hat{\sigma}_{\mathrm{gA}}$ |
|---|---|---|---|
| 3.84 | 0.019 | 0.17 | 0.010 |
| 3.96 | 0.076 | 0.14 | 0.008 |

Table 7.1: The *UA*-value and *gA*-value estimates 30 minutes sample period, together with the estimated standard deviances $\sigma_{\mathrm{UA}}$ and $\sigma_{\mathrm{gA}}$.

## 7.3 Comparison of all models

In this section the results from applying all models on 30 minutes values for both CE3 and CE4 are presented. The $UA$ and $gA$ estimates are shown with 95% confidence bands in Figure 7.4. First it is noted that all the models give very reasonable

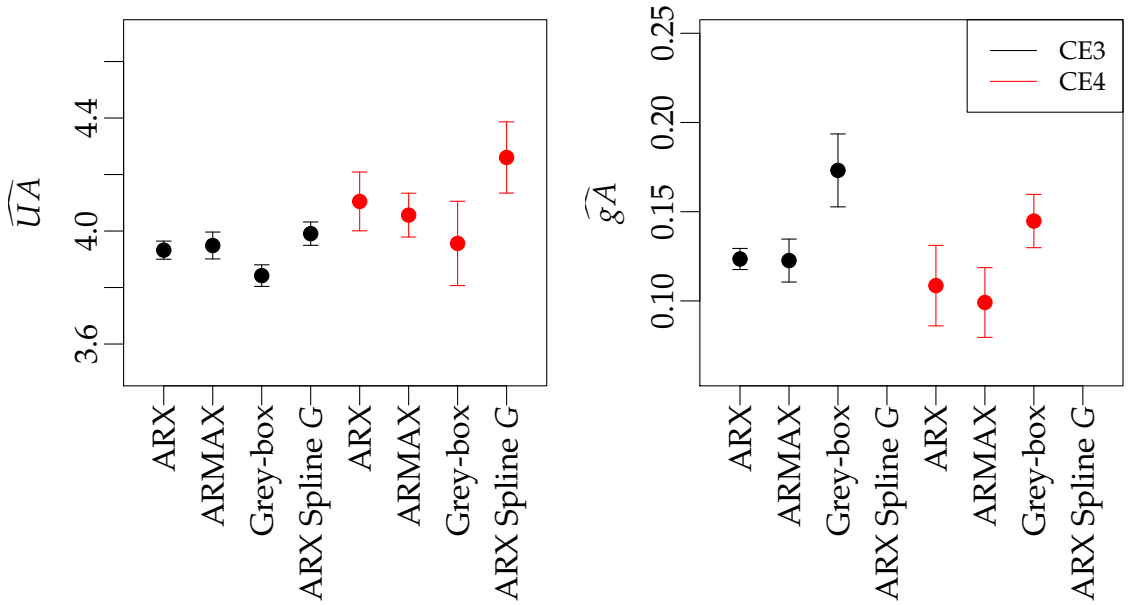


Figure 7.4: Estimates with 95% confidence bands for 30 minutes values.

estimates, however there are some differences. Clearly there is a tendency for increasing $UA$-values for CE4 compared to CE3, as noted before this could have a physical explanation or be caused by correlation of the inputs. It is also very clear that the $UA$-value for the splined model is significantly higher. This could be because the absorbtion of radiation is taken better into account, which in this case means that more radiation is absorbed, which then naturally cause the $UA$-value to increase, because more thermal energy needs to flow out of the box.

## 7.4 Simulation of Series 6

The indoor temperature which is missing from Series 6 is simulated with the selected grey-box model, $Model_{\text{TiTw.GinTw}}$. The simulation is an $n$-step deterministic prediction. In Figure 7.5 the simulated indoor temperature for Series 5 is plotted, in order to see how well the simulations fits to the measurements. Clearly the fit from CE4 matches very well the measured indoor temperature, whereas the fit from CE3 slips a bit away from the measurements and has some fast fluctuations.

In Figure 7.6 the simulated indoor temperature for Series 6 is shown. Since no initial temperature is given in the CE4 instructions document, it is set to 29 °C for both the indoor and wall temperature.

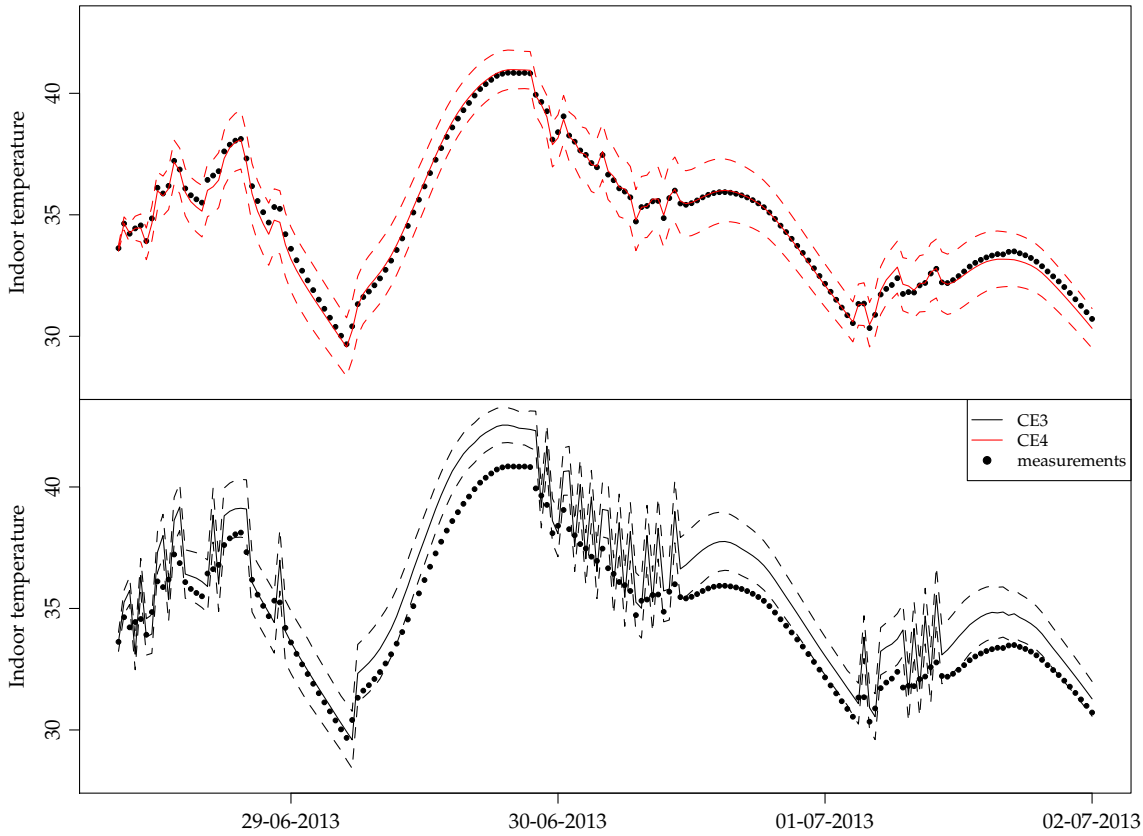


Figure 7.5: Simulations of indoor temperature for Series 5 using the selected grey-box model. Both the fit from CE3 and CE4 is plotted together with their estimated 95% confidence bands.

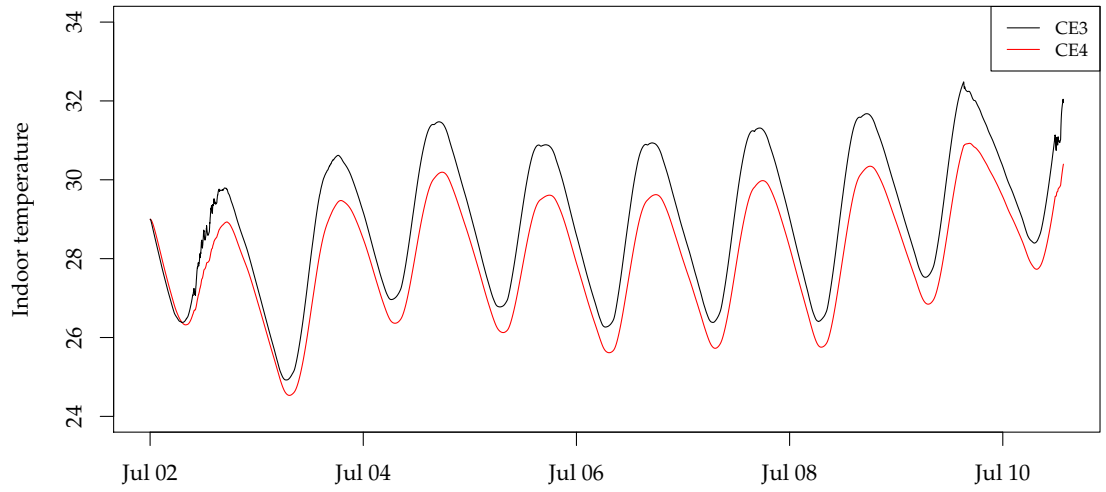


Figure 7.6: Simulation of the indoor temperature in Series 6. Both the fit for CE3 and CE4 is plotted.

# Chapter 8

# Discussion and conclusion

In this section a discussion and conclusions are outlined. First recommendations for further experiments are given.

## 8.1 Recommendations for improvements of the experiments

The experiment Series 4 and Series 5 should be repeated in the future experiments with test box. The following recommendations are given based on the experience gained working with the current data:

- Faster sampling or averaging (integration) of the heating signal to achieve a better resolution for the co-heating experiment.
- At least as detailed solar radiation measurements: north faced vertical global radiation, beam radiation, global diffuse radiation, global radiation.
- Another dynamic test sequence with some smoothed transients to avoid the complex behavior which occurs when the heat is switch on/off and fewer of the fast switching periods.
- Important to have both clear-sky and cloud-sky days in the data, however this cannot be controlled, but to some extend it would be very good to keep on each the experiment until different solar radiation excitement is included in the data, if possible.

## 8.2 Discussion

In this section a discussion of the results and suggestions for further work are given:

- The ARX and ARMAX model selection procedure is simplified and further work could investigate the use of other model selection strategies. For example the use of: likelihood-ratio tests, AIC, forward and backward selection or other techniques. Actually several of the strategies was tried, but no clear and stable approach was found. Furthermore, Ridge estimation could be considered to compensate for the cross-correlation of the lagged values.

- For the ARMAX models it is a bit surprising why the use of $B_i$ polynomials with order zero gives more stable estimates, since this essentially means that the dynamical response from the external temperature and solar radiation is the same with only the magnitude as the difference. This should be studied further.
- It could be interesting to fit ARX and ARMAX models to the Series 5 Rolbs data using the indoor temperature as model output.
- Differences between the CE3 and CE4 experiment is evident:
  - The external temperature and the solar radiation are more correlated in the CE4 data, hence also the $UA$ and $gA$ are better separated.
  - The signal to noise ratio is lower in the CE Series 4 compared to the similar CE3 25C experiment, due to the on/off quantification error described in Section 2.1. Which could be the cause for the higher uncertainty of the estimates found using CE4 compared to CE3.
- In a future data set it would be valuable to have days where clouds appear partly and generate fast transients in the solar radiation signal. This would allow for more details on the dynamic response to solar radiation to be inferred, which also would make it more possible to separate the effect of diffuse and direct solar radiation better.
- The increase in $UA$ value for CE4 from using an enhanced description of the solar radiation effects is found quite interesting, especially because this increase did not occur with the same magnitude for CE3. Hence this indicate that this is caused by some difference between the experiments, maybe the explanation is that the inputs are correlated or it is due to some physical phenomenon of the different climate conditions.

## 8.3 Conclusion

The applied models and the proposed model selection procedure and evaluation enables estimation of the essential thermal performance parameters, $UA$ and $gA$ values, for the test box, including their associated uncertainties. The ARX, ARMAX and SDE based grey-box models all gives estimates, which are in similar range and with overlapping 95% confidence bands. Models for a semi-parametric description of the solar radiation effect are presented. These models provide, with no prior information except the location of the box, an enhanced description of the effect of solar radiation. Using these models the $UA$-value estimate increases slightly, and these models should be further studied and compared to models where more prior information is used, preferably using data containing periods with both cloudy (only diffuse radiation) and clear-sky days, to gain more knowledge on the advantages of different ways to detail the description of the solar radiation effects. Grey-box models which include shifting levels of system noise is presented, such models provide a very useful way of dealing with data where some periods have a higher level of unknown disturbances, for example where people are in a building only in certain periods. A more detailed description of the solar radiation entering the outer surfaces for grey-box models should be studied in further work.

# Bibliography

P. Bacher and P. Delff. Iea common exercise 3: Arx models for thermal performance characterization based on constant indoor temperature experiments. Technical report, DTU Compute, 2013.

P. Bacher and H. Madsen. Identifying suitable models for the heat dynamics of buildings. *Energy & Buildings*, 43(7):1511–1522, 2011. ISSN 03787788. doi: 10.1016/j.enbuild.2011.02.005.

C. De Boor, K. Höllig, and S. D. Riemenschneider. *Box splines*, volume 98. Springer, 1993.

M. Jiménez, H. Madsen, and K. Andersen. Identification of the main thermal characteristics of building components using MATLAB. *Building and Environment*, 43 (2):170–180, 2008. ISSN 03601323, 1873684x. doi: 10.1016/j.buildenv.2006.10.030.

N. R. Kristensen, H. Madsen, and S. B. Jørgensen. Parameter estimation in stochastic grey-box models. *Automatica*, 40(2):225–237, 2004. ISSN 0005-1098. doi: DOI:10.1016/j.automatica.2003.10.001.

H. Madsen and J. Holst. Estimation of continuous-time models for the heat dynamics of a building. *Energy and Buildings*, 22(1):67–79, 1995. ISSN 03787788.

R Core Team. *R: A Language and Environment for Statistical Computing*. R Foundation for Statistical Computing, Vienna, Austria, 2013. URL `http://www.R-project.org/`.

J. Ruiz-Arias, H. Alsamamra, J. Tovar-Pescador, and D. Pozo-Vázquez. Proposal of a regressive model for the hourly diffuse solar radiation under all sky conditions. *Energy Conversion and Management*, 51(5):881–893, 2010. ISSN 01968904. doi: 10.1016/j.enconman.2009.11.024.